Cancer
Research

LKB1 and KEAP1/NRF2 Pathways Cooperatively Promote Metabolic Reprogramming with Enhanced Glutamine Dependence in *KRAS*-Mutant Lung Adenocarcinoma

Ana Galan-Cobo[1], Piyada Sitthideatphaiboon[2], Xiao Qu[3], Alissa Poteete[1], Marlese A. Pisegna[1], Pan Tong[4], Pei-Hsuan Chen[5], Lindsey K. Boroughs[6], Mirna L.M. Rodriguez[7], Winter Zhang[7], Francesco Parlati[7], Jing Wang[4], Varsha Gandhi[8], Ferdinandos Skoulidis[1], Ralph J. DeBerardinis[9], John D. Minna[10], and John V. Heymach[1]

Abstract

In *KRAS*-mutant lung adenocarcinoma, tumors with LKB1 loss (KL) are highly enriched for concurrent *KEAP1* mutations, which activate the KEAP1/NRF2 pathway (KLK). Here, we investigated the biological consequences of these cooccurring alterations and explored whether they conferred specific therapeutic vulnerabilities. Compared with KL tumors, KLK tumors exhibited increased expression of genes involved in glutamine metabolism, the tricarboxylic acid cycle, and the redox homeostasis signature. Using isogenic pairs with knockdown or overexpression of LKB1, KEAP1, and NRF2, we found that LKB1 loss results in increased energetic and redox stress marked by increased levels of intracellular reactive oxygen species and decreased levels of ATP, NADPH/NADP$^+$ ratio, and glutathione. Activation of the KEAP1/NRF2 axis in LKB1-deficient cells enhanced cell survival and played a critical role in the maintenance of energetic and redox homeostasis in a glutamine-dependent manner. LKB1 and the KEAP1/NRF2 pathways cooperatively drove metabolic reprogramming and enhanced sensitivity to the glutaminase inhibitor CB-839 *in vitro* and *in vivo*. Overall, these findings elucidate the adaptive advantage provided by KEAP1/NRF2 pathway activation in KL tumors and support clinical testing of glutaminase inhibitor in subsets of KRAS-mutant lung adenocarcinoma.

A, *KRAS*-mutant tumors use glucose or glutamine to fuel their metabolism, while *KRAS*/LKB1/*KEAP1* mutant tumors preferentially use glutamine. B, Blocking glutaminolysis using GLSi impairs proliferation of *KRAS*/LKB1/*KEAP1*-mutant tumors as they are unable to maintain the TCA cycle.

© 2019 American Association for Cancer Research

Cancer Research

Significance: In *KRAS*-mutant non–small cell lung cancer, LKB1 loss results in enhanced energetic/redox stress, which is tolerated, in part, through cooccurring KEAP1/NRF2–dependent metabolic adaptations, thus enhancing glutamine dependence and vulnerability to glutaminase inhibition.

Graphical Abstract: http://cancerres.aacrjournals.org/content/canres/79/13/3251/F1.large.jpg.
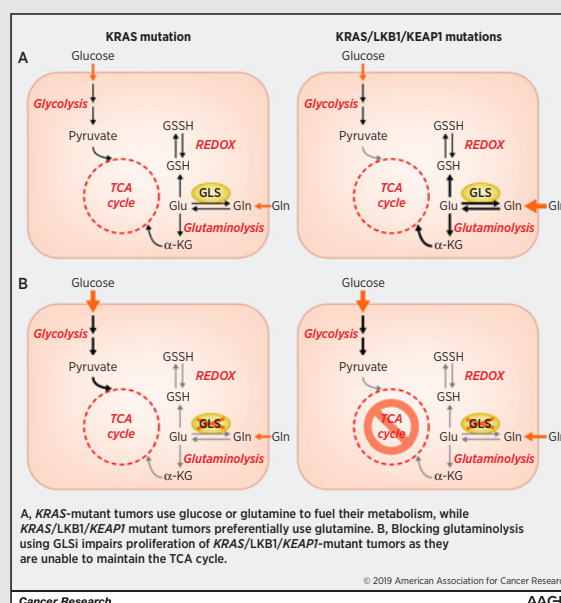
[1]Department of Thoracic, Head and Neck Medical Oncology, The University of Texas MD Anderson Cancer Center, Houston, Texas. [2]Department of Medicine, Division of Medical Oncology, Chulalongkorn University-King Chulalongkorn Memorial Hospital, Bangkok, Thailand. [3]Institute of Oncology, Shandong Provincial Hospital, Shandong University, Jinan, P.R. China. [4]Department of Bioinformatics and Computational Biology, The University of Texas MD Anderson Cancer Center, Houston, Texas. [5]Department of Medical Oncology, Dana-Farber Cancer Institute, Boston, Massachussets. [6]19946 Hibiscus Dr., Jupiter, Florida. [7]Calithera Biosciences, South San Francisco, California. [8]Department of Experimental Therapeutics, The University of Texas MD Anderson Cancer Center, Houston, Texas. [9]Eugene McDermott Center for Human Growth & Development, Children's Medical Center Research Institute at UTSW, Department of Pediatrics, UT Southwestern Medical Center, Dallas, Texas. [10]Hamon Center for Therapeutic Oncology Research and Simmons Cancer Center, The University of Texas Southwestern Medical Center, Dallas, Texas.

Corresponding Author: John V. Heymach, The University of Texas MD Anderson Cancer Center, M.D. Anderson Cancer Center, Unit 432, 1515 Holcombe Blvd, Houston, TX 77030. Phone: 713-792-6363; Fax: 713-792-1220; E-mail: jheymach@mdanderson.org

Introduction

KRAS is the most commonly mutated oncogenic driver in non–small cell lung cancer (NSCLC) and other solid tumors. A major obstacle for developing an effective treatment strategy for these tumors is heterogeneity in the biology, downstream signaling, and therapeutic responsiveness of the tumors (1). Serine/threonine kinase *STK11* (LKB1) is the second most commonly altered tumor suppressor in NSCLC (2, 3). *STK11* mutations or genomic loss frequently cooccur with *KRAS* alterations (4), and this combination results in a highly aggressive phenotype and reduced survival rates in both preclinical models (5) and patients with NSCLC (4). Although LKB1 loss occurs more frequently than genomic alterations in *EGFR, ALK, ROS, RET,* and *BRAF* combined in NSCLC, there are currently no treatment strategies specific for LKB1-deficient NSCLC.

LKB1 directly phosphorylates and activates AMPK, which works as a master sensor of cellular energy (6). In response to energetic stress, AMPK alters the cellular metabolism to restore ATP levels and regulates NADPH concentrations (7). In addition, AMPK regulates the activity of mTOR, a key driver of cellular growth and proliferation (8). Thus, under conditions of energetic stress, the LKB1–AMPK axis plays a critical role in modulating cell growth and proliferation to maintain adequate ATP and NADPH levels. Tumors bearing LKB1 loss (KL) demonstrate evidence of high redox and energetic stress, likely due, at least in part, to low levels of NADPH and an inability to maintain ATP homeostasis. As a consequence of increased energetic and metabolic stress, LKB1-deficient cells generate elevated levels of reactive oxygen species (ROS; ref. 9).

We previously reported that *KEAP1*-inactivating mutations frequently cooccur in KL tumors (4). Given the role of KEAP1 as a negative regulator of NRF2-mediated antioxidant expression (10), we hypothesized that the increased ROS levels present in LKB1-deficient tumors drive a positive selection pressure for KEAP1 loss because this provides protection against ROS-mediated damage via upregulation of NRF2 target genes. Thus, KL tumors with additional activation of KEAP1/NRF2 pathway (KLK) are particularly resistant to high ROS accumulation within the tumor microenvironment.

Glutamate-cysteine ligase (*GCLC*) is a NRF2-regulated gene that catalyzes the production of glutathione (GSH), a ROS detoxicant, from glutamate. Glutamine is one of the main precursors for glutamate and, consequently, for GSH synthesis, and complements glucose's contribution to the tricarboxylic acid (TCA) cycle in the absence of glucose. Cancer cells frequently shift their metabolism to be more glutamine-dependent, and therefore glutaminase, the enzyme that converts glutamine to glutamate, has emerged as a potential therapeutic target (11–17). Deregulation of the KEAP1/NRF2 axis was recently reported to alter metabolic requirements, rendering lung tumor cells more sensitive to glutamine metabolism inhibitors (18). Therefore, KLK tumors are likely vulnerable to therapies that target NRF2-mediated ROS detoxification, and glutaminase is a potential target to block either antioxidant pathways or metabolic progression. Given these observations, we hypothesized that KLK NSCLC cells are vulnerable to glutaminase inhibition.

In this study, we evaluated the impact of *KEAP1* comutations in KL NSCLC tumor cells and investigated whether LKB1 and KEAP1/NRF2 signaling pathways together contribute to a specific therapeutic vulnerability to energetic and ROS stress induction.

Using bio-informatics, *in vitro*, and *in vivo* approaches, we determined that loss of KEAP1 provides an adaptive advantage for tumors with functional inactivation of the LKB1–AMPK axis undergoing energetic and oxidative stress, providing a potential explanation for the increased frequency of KEAP1/NRF2 alterations in KL tumors. In addition, we showed how this positive selective pressure drives metabolic reprogramming in KLK tumors, making them specifically sensitive to glutamine metabolism blocking. Collectively, our data indicate that in KLK tumors, both LKB1 and KEAP1/NRF2 pathways cooperatively induce sensitivity to glutaminase inhibition, suggesting that glutaminase inhibition is a promising treatment strategy for NSCLC harboring this specific genetic background.

Materials and Methods

Cell culture

Fingerprinting and *Mycoplasma* test (MycoAlert Mycoplasma Detection Kit) were performed periodically to authentication.

Three cell lines with *KRAS, STK11*/LKB1, and *KEAP1* comutations (A549, H460, and H2030), one cell line with *KRAS* and *STK11*/LKB1 comutations (H23), and one cell line with no mutations (Calu-6) were used. All cell lines were obtained from the ATCC. All cells were maintained in RPMI1640 medium (Sigma) supplemented with 10% FBS, 1% glutamine, and 1% penicillin–streptomycin.

Murine cell lines

LKR13 cell line was derived by serial passage of minced lung adenocarcinoma tissues from *Kras*[LA1] mice (19). The cells were cultured in RPMI1640 supplemented with 10% FBS (Invitrogen). *KRAS*-mutant isogenic pairs for *STK11*/LKB1 (KL), *KEAP1* (KK), or both (KLK), were generated using CRISPR/Cas9 System (Santa Cruz Biotechnology). A list of abbreviations with description for isogenic pairs is included in Supplementary Table S1.

siRNA transfection

For siRNA transfections, A549 cells were transfected with siRNA-targeting NRF2 and control siRNA at a final concentration of 100 nmol/L using Dharmafect 1 Transfection Reagent (Dharmacon). Protein was isolated after 72 hours.

Viral infection

Stable overexpression of LKB1 in A549, H460, H23, and H2030 cells and stable shRNA-mediated LKB1 knockdown in Calu-6 were established by lentiviral transduction using a viral vector system. Viral particle production was performed by cotransfecting viral vectors with lentiviral-packaging plasmids (psPAX2 and pMD2.G) into 293T cells using Lipofectamine 2000 Reagent with PLUSTM Reagent (Life Technologies). Three days after transfection, supernatant was collected and concentrated using PEG-itTM Virus Precipitation Solution (System Biosciences) overnight at 4°C, according to the manufacturer's protocol. Cell lines were then incubated with the supernatant containing viral particles supplemented with 8 µg/mL polybrene (Sigma) at 37°C overnight. To establish single clones, we sorted infected cells using single-cell sort GFP-expressing cells. Single clones were maintained and expanded with medium containing 2 µg/mL puromycin (Gibco, Thermo Fisher Scientific). After expansion, the cells were maintained in regular medium.

Western blot analysis

Cell pellet was washed with cold PBS once and then lysed with a variable volume of ice-cold lysis RIPA buffer (1% Triton X-100, 50 mmol/L HEPES, pH 7.4, 150 mmol/L NaCl, 1.5 mmol/L $MgCl_2$, 1 mmol/L EDTA, 100 mmol/L NaF, 10 mmol/L Na pyrophosphate, 1 mmol/L Na_3VO_4, 10% glycerol, supplemented immediately prior to cell lysis with 1 mmol/L phenylmethylsulfonyl fluoride, complete protease inhibitor, and phosSTOP phosphatase inhibitor cocktail; Roche Applied Science. Lysates were centrifuged at 14,000 rotations per minute for 15 minutes at 4°C, and then cleared supernatant was collected and protein concentration was quantified using the colorimetric Bio-Rad Protein Assay Dye Reagent Concentration (Bio-Rad), according to the manufacturer's protocol. Next, 20–25 μg of total protein was loaded and resolved in 4%–20% precast gradient gels (Bio-Rad) and transferred to polyvinylidene difluoride membranes using the Trans-Blot Turbo transfer system and Trans-Blot Turbo RTA Transfer Kit (Bio-Rad), according to the manufacturer's protocol. Membranes were blocked in 5% nonfat dry milk (Bio-Rad) in 0.1% TBS-Tween (150 mmol/L NaCl, 10 mmol/L Tris-HCL, pH 8) for 1 hour at room temperature and incubated with the following primary antibodies with 0.1% goat serum plus 2 mmol/L EDTA dissolved in 0.1% TBS-Tween: LKB1(27D10), 1:1,000, #3050 (Cell Signaling Technology); KEAP1 (H436), 1:1,000, #4617 (Cell Signaling Technology); NRF2 (EP1808Y), 1:1,000, ab62352 (Abcam); NQO1 (A180), 1:1,000, #3187 (Cell Signaling Technology); GCLC, 1:1,000, ab41643 (Abcam); GAPDH (14C10), 1:1,000, #2118 (Cell Signaling Technology); Vinculin, 1:5,000 (Abcam); β-actin, 1:5,000 (Abcam). Membranes were washed briefly with 0.1% TBS-Tween and then incubated with horseradish peroxidase–conjugated secondary antibodies at a concentration of 1:3,000 in 2.5% nonfat dry milk for 1 hour at room temperature. Signal was developed with SuperSignal West Pico PLUS Chemiluminescent Substrate (Thermo Fisher Scientific) detection reagents.

Sulforhodamine B colorimetric assay

Cell proliferation was assessed using the sulforhodamine B (SRB) assay, as described previously (20). Briefly, cells were seeded in 96-well plates at 2,000 cells per well. After an incubation period with indicated drugs, cell monolayers were fixed with 10% (wt/vol) trichloroacetic acid for 1 hour at 4°C. The fixed cells were stained with SRB (0.4%) for 30 minutes at room temperature, after which, the excess dye was removed by washing repeatedly with 1% (vol/vol) acetic acid. The protein-bound dye was dissolved in 10 mmol/L Tris base solution for optical density determination at 560 nm using a microplate reader.

Cell counting assay

Cells were seeded in 6-well plate. Twenty-four hours later, CB-839 and DMSO were added at the indicated concentrations. After incubation periods with indicated drugs, cells were harvested and stained with Trypan Blue 0.4% and counted using Count II Automatic Cell Counter (Invitrogen).

Cell viability assay and IC_{50} estimation

IC_{50} was estimated using the CellTiter-Glo Luminescent Cell Viability Assay (Promega), according to the manufacturer's protocol. When cells were in the exponential growth phase, the cells were detached and counted using a Countess Automated Cell Counter (Invitrogen). An optimized number of viable cells for each cell line were then plated in polybase white 384-well plates (Greiner Bio-One), in triplicate for each experimental condition. Cells were allowed to attach, depending on the cell line, for between 8 hours and overnight and subsequently exposed to seven different concentrations of glutaminase inhibitor (serial 3-fold dilutions) in a final volume of 40 μL of media per well. Plates were spun at $300 \times g$ for 30 seconds to ensure even addition of the drug, and plates were then incubated for an additional 72 hours. Next, 11 μL of CellTiter-Glo reagent was added to each well, and contents were briefly mixed and incubated for 15 minutes. Bioluminescence was measured using a FLUOstar OPTIMA Multimode Microplate Reader (BMG Labtech). Average readings from triplicate wells were then expressed as a percentage of average bioluminescence measured from control DMSO wells treated with vehicle (DMSO) at a concentration of 0.347% (v/v), representing the highest DMSO concentration in drug-treated cells. A dose–response model was used to estimate IC_{50} values from cell viability data. Multiple models from the DoseFinding and drc packages were fitted and the best model was selected on the basis of residual SE using the R software.

Relative cell loss or proliferation in the presence of 1 μmol/L CB-839 or in glutamine-free media was determined by comparing the CTG signals measured at time (t) = 72 hours under experimental conditions (CTG_{exp_72}) with both the CTG signal at t = 72 hours for vehicle (DMSO)-treated cells (CTG_{DMSO_72}) and the CTG signal measured at t = 0, the time of CB-839 addition or glutamine withdrawal (CTG_0), using the following equations:% cell loss (when $CTG_{exp\_72} < CTG_0$) = $100 \times (CTG_{exp\_72} - CTG_0)/CTG_0$;% cell proliferation (when $CTG_{exp\_72} > CTG_0$) = $100 \times (CTG_{exp\_72} - CTG_0)/(CTG_{DMSO\_72} - CTG_0)$.

Clonogenic survival assays

Exponentially growing cells were plated in duplicate at three dilutions into 6-well plates containing 2 mL of medium. Cells were incubated for 24 hours in a humidified CO_2 incubator at 37°C, and subsequently different drugs were added into the medium for 4 hours. The medium was then replaced with fresh medium, allowing cells to continuously grow for colony formation for 10 to 14 days. To assess clonogenic survival, we stained cells with 1% crystal violet.

Measurement of ROS levels

To measure endogenous ROS levels, we incubated cells with 20 μmol/L 2′, 7′-dichlorodihydrofluorescein diacetate (Cellular Reactive Oxygen Species Detection Assay Kit; Abcam) for 30 minutes at 37°C and ROS-mediated oxidation of the fluorescent compound DCF was measured. Fluorescence of oxidized DCF was measured at an excitation wavelength of 488 nm and an emission wavelength of 535 nm using a FACS Scan flow cytometer (BD Biosciences). Alternatively, cells were stained with CellROX Deep Red Probe (Invitrogen) according to the manufacturer's protocol.

ATP measurement

Cells were initially plated into a 96-well plate at 8,000 cells per well. The following day, indicated drugs were added into the cell medium. After the indicated time, cells were processed according to the manufacturer's protocol (ATPlite, PerkinElmer). All the plates were screened by the BMG reader for luminescence signal. The ATP concentration was normalized to protein concentration.

Annexin V/7-AAD staining

Annexin V assays were performed according to the manufacturer's protocol (BD Biosciences). Briefly, 1×10^5 cells were plated into 6-well plates and allowed to adhere overnight before incubation in the presence or absence of indicated reagents. The cells were harvested and incubated with 5 μL of PE-conjugated Annexin V and 5 μL of 7-AAD for 15 minutes at room temperature in the dark. Fluorescence analyses were performed using FACS Scan Flow Cytometry (BD Biosciences). Cells were classified as early apoptotic (Annexin V–positive/7-AAD–negative), late apoptotic/necrotic (Annexin V–positive/7-AAD–positive), necrotic/dead (Annexin V–negative/7-AAD–positive), and live (Annexin V–negative/7-AAD–negative).

Cell-cycle analysis

Cell cycle was analyzed by determining bromodeoxyuridine incorporation compared with DNA content. A total of 3×10^5 cells were initially plated into a 60-mm plate. The following day, drugs at indicated concentrations were added into the cell medium. After the indicated time, cells were processed according to the manufacturer's protocol (BD Biosciences). Cell cycle was also analyzed by DNA content. Cells with or without treatment were trypsinized and fixed with 70% ethanol at $-20°C$ overnight. DNA was labeled with propidium iodide (BD Biosciences) at $37°C$ for 15 minutes. Approximately 10,000 cells were collected for each assay and analyzed using FACS Scan Flow Cytometry (BD Biosciences).

Metabolite measurements

A total of 4×10^5 cells were plated into a 60-mm plate for glutamate measurement or 4,000 cells were plated into a 96-well plate for GSH or NADPH/NADH$^+$ measurement. Glutamate levels were measured using the Glutamate Assay Kit (ab83389; Abcam) according to the manufacturer's protocol. GSH/GSSG and NADPH/NADP were measured using the GSH-Glo Assay Kit (Promega) or NADPH/NADP-Glo Assay Kit (Promega), according to the manufacturer's protocol. All metabolite concentrations were normalized to protein concentration.

Rescue experiments

All nucleotides were added at final concentration of 100 μmol/L. Glucose was added at final concentration of 10 or 5 g/L. Pyruvate, α-Ketoglutarate, glucose-6-phosphate, fructose-6-phosphate, and fructose 1–6-biphosphate were added at a final concentration of 1 mmol/L. All amino acids were added at a final concentration of 2 mg/mL.

Metabolic analysis

A549 cells were plated at 4.5×10^6 cells per 10-cm dish and H727 cells were plated at 8.0×10^6 cells per dish 24 hours prior to treatment. Cells were treated on day 0 with 0.01% DMSO, or 1 μmol/L of CB-839 for 24 hours. On day 1, 2 hours prior to harvest, samples were washed with 5-mL media containing 10% dialyzed FBS. Ten milliliters of media was added to plates and plates were returned to the incubator for 2 hours. Media was then aspirated from plates and 4 mL of 80% chilled MeOH ($-80°C$) was immediately added. Plates were incubated at $-80°C$ for 15 minutes. Cells were then scraped with cell scraper to release cells while keeping plates on dry ice. The MeOH/cell lysate mixture was collected and transferred to conical tubes on dry ice. Tubes were centrifuged at full speed in $4°C$ chilled centrifuge for 5 minutes.

Supernatant was transferred to another set of conical tubes on dry ice by decanting. The remaining pellet was resuspended in 500 μL of cold MeOH and the mixture was moved to a microcentrifuge tube. Microcentrifuge tubes were spun at full speed for 5 minutes in $4°C$ chilled microcentrifuge. Supernatant was transferred to conical tube with previously collected supernatant and this step was repeated two times. One milliliter of collected supernatant was transferred to prelabelled sample/submission tubes and dried by speedvac. Samples were then submitted to the Beth Israel Deaconess Medical Center Mass Spectrometry core facility for analysis by LC/MS-MS using an Agilent SCIEX 5500 QTRAP to profile 258 metabolites (21). A list of abbreviations for analyzed metabolites is included in Supplementary Table S1.

Drugs

CB-839 (EMD Millipore) was resuspended in DMSO to a final concentration of 10 mmol/L. Drug aliquots were stored at $-80°C$ and each aliquot was used only once.

Animals and tumor xenografts

Female nude mice (NCI-nu, 4–8 weeks old) were obtained from the Animal Production Area of the NCI (Frederick Cancer Center, Frederick, MD) and housed in facilities approved by the Association for Assessment and Accreditation of Laboratory Animal Care International and used and maintained under pathogen-free conditions in facilities approved by the American Association for Accreditation Laboratory Animal Care and in accordance with current regulations and standards of the U. S Department of Agriculture, the U. S. Department of Health and Human Services, and the NIH approved by the Association for Assessment and Accreditation of Laboratory Animal Care International. A total of 5×10^6 subconfluent A549-CTR and A549-KEAP1 tumor cells were injected in to the dorsal flank and growth was monitored weekly. When the tumor reached 250–350 mm^3 the animals were randomized to the respective treatment groups. Mice were treated with CB-839 200 mpk, by oral gavage, every 12 hours. Tumor volumes were measured every 3 days.

NSG female mice (Jackson Labs) were implanted with serially transplanted tumor sections from isolated patient derived xenografts (PDX) into a single flank with Matrigel and allowed to grow to an average volume of 100 mm^3 as monitored by caliper measurements. After two consecutive measurements showing growth, animals were randomized into groups of 8 and treated with CB-839 at 200 mpk, twice a day, orally for 27 days on a 5on/2off schedule. Mice were between six- and 8-week old. Tumor volume was calculated using the formula: $V = l^{2*}L/2$ (l length; L width). Tumor volumes were measured every 3 days.

Statistical analysis

Statistical analyses were conducted using GraphPad Prism version 6.00 for Windows (GraphPad Software; www.graphpad.com) or the R system for statistical computing. An unpaired t test was used to compare the mean of two different groups when the distribution of the population was normal. One-way ANOVA was used to compare the means of three or more groups under the assumption of normal distribution, and the Tukey posttest was applied for multiple comparisons. The nonparametric Mann–Whitney U test and Kruskal–Wallis H test were used to compare the mean ranks between two groups (U test) or three groups (H test). The Fisher exact test was used for the analysis of contingency

tables. All P values were two-tailed and for all analyses, $P \leq 0.05$ is considered statistically significant, unless otherwise specified.

Results

The KEAP1/NRF2 axis is essential for maintaining ATP levels and redox homeostasis in *KRAS*-mutant KL tumors

We performed bioinformatic analysis incorporating transcriptional and mutational data for *KRAS*-mutant lung adenocarcinoma from The Cancer Genome Atlas (TCGA) database. We observed significant cooccurrence of *KEAP1* mutations and *STK11*/LKB1 loss (Fisher exact test, $P < 0.001$). In particular, 37.4% of *STK11*/LKB1–loss samples had concurrent *KEAP1* comutations, whereas only 1.3% of wild-type *STK11*/LKB1 samples had a *KEAP1* comutation (Fig. 1A), demonstrating strong enrichment of *KEAP1* mutations in *STK11*/LKB1–loss samples. This enrichment of *KEAP1* mutations also occurred in tumors with *STK11*/LKB1 loss and wild-type *KRAS* (Fig. 1A).

To determine whether *KRAS*-mutant lung adenocarcinoma samples (K tumors) with loss of *STK11*/LKB1 (KL tumors) or both *STK11*/LKB1 loss and comutation of *KEAP1* (KLK tumors) exhibit a specific type of metabolic reprogramming, we ran a supervised analysis for selected genes comparing K, KL, KK, and KLK subsets. We analyzed the expression of genes involved in glycolysis, glutamine metabolism, the NRF2 pathway, the pentose phosphate pathway (PPP), the TCA cycle, fatty acid metabolism, and others. The KLK subset demonstrated a markedly differential expression of metabolic genes compared with the K, the KL, or the KK subset, most notably in genes related to glutamine metabolism and the TCA cycle. Seventy-four metabolic genes with statistically significant differential expression were found in the KLK subset when compared with the K subset (Fig. 1B). Analysis of the KL subset also displayed a substantial number (54) of metabolic genes significantly altered when compared with the K subset. Moreover, when the KK subset was compared with the KLK cohort, we observed 52 metabolic genes altered, supporting the contribution of *STK11*/LKB1 loss (in the absence of *KEAP1*/NRF2 pathway activation) in tumor cell metabolic reprogramming (Supplementary Fig. S1A and S1B). Our analysis comparing the KK subset with K subset showed a smaller number (20) of metabolic genes significantly altered (Supplementary Fig. S1C), while comparative analysis of KL subset versus KLK subset displayed 48 genes significantly altered (Supplementary Fig. S1D). These data suggest that in *KRAS*-mutant tumors, *STK11*/LKB1 loss has a significant impact over glutaminolysis as well as NRF2 and TCA cycle among others. Indeed, coalterations of *STK11*/LKB1 and *KEAP1* showed a greater association with modifications in the metabolic and redox phenotype.

Consistent with this observation, gene set enrichment analysis showed that expression signatures related to glutamine, nitrogen species metabolic process, TCA cycle, and pyruvate metabolism were significantly enriched in the KLK subset when compared with the K subset (Fig. 1C; Supplementary Fig. S2). Supporting the impact of *STK11*/LKB1 loss on metabolic reprogramming, K versus KL and KK versus KLK comparisons showed enrichment of TCA cycle, glutamine metabolism, and redox homeostasis gene signatures when compared with K subset (Supplementary Fig. S2A). Statistically significant enrichment related gene signatures were not found in KK versus K subset analysis.

To directly study the regulation of energetic and ROS stress in KL NSCLC, we used A549 NSCLC cells, which harbor a *KRAS* mutation, LKB1 deficiency, and a *KEAP1*-inactivating mutation (KLK). Reexpression of LKB1 did not modify cell proliferation (Fig. 2A and B) but did significantly increase ATP levels, while reducing ROS levels and the NADPH/NADP$^+$ ratio (Fig. 2C) consistent with a role for LKB1 in promoting energetic and redox stress. Levels of phosphorylated AMPK, a target of LKB1, were higher in LKB1-expressing cells, indicating that the expressed LKB1 protein was functional (Fig. 2A).

Because KEAP1 is a negative upstream regulator of the antioxidant transcription factor NRF2 and can also be directly regulated by ROS, we examined the expression NRF2 in LKB1-deficient and -proficient cells using Western blot analysis. A549 cells expressing the control vector expressed high levels of NRF2, whereas reexpression of LKB1 reduced NRF2 levels (Fig. 2D), indicating an interaction between these pathways. Similar results were observed with two additional isogenic pairs, Calu6 and H460 (Supplementary Fig. S3A). siRNA-mediated downregulation of NRF2 resulted in decreased expression of the NRF2 target genes *GCLC* and *NAD(P)H quinone dehydrogenase 1* (*NQO1*; Fig. 2E) and decreased cell number (Fig. 2F; Supplementary Fig. S3B). Moreover, shRNA-mediated downregulation of NRF2 resulted in deregulation of cellular redox homeostasis, indicated by reduced levels of GSH, increased levels of ROS, and a reduced NADPH/NADP$^+$ ratio compared with the A549 control cells (Fig. 2G).

Because NRF2 is an important modulator of ROS levels, we next evaluated the effect of LKB1 expression and NRF2 downregulation on sensitivity to induction of ROS stress. Assessment of the apoptotic rate based on Annexin-V/7-ADD staining revealed that ROS stress induced by treatment with H_2O_2 (400 μmol/L) induced greater levels of apoptosis in cells reexpressing LKB1 or downregulating NRF2 than in control A549 cells (Fig. 2H). Similar results were obtained using lower or higher concentrations of H_2O_2 or overexpressing KEAP1 (Supplementary Fig. S3C). These data suggest that LKB1 loss leads to upregulation of the KEAP1/NRF2 axis, which is important for the maintenance of redox homeostasis and resistance to oxidative stress in LKB1-deficient cells in *KRAS*-mutant NSCLC.

Glutaminase inhibition blocks cell proliferation and increases energetic and oxidative stress sensitivity in KL tumor cells

Because KL tumors exhibit deregulation of the KEAP1/NRF2 pathway, which promotes ROS detoxification, in part, by upregulating the expression of the GCLC enzyme and, in turn, GSH production (Fig. 3A), we hypothesized that KL tumors have increased glutamine dependence to maintain a proper cellular ROS balance. To investigate this, we screened NSCLC cell lines for sensitivity to the glutaminase inhibitor CB-839 and glutamine withdrawal (Fig. 3B). Most cell lines that displayed high glutaminase inhibitor sensitivity harbored comutations in *STK11*/LKB1 and *KEAP1* genes. The same trend was observed regarding glutamine withdrawal sensitivity. One KLK cell line, H1355, did not show high sensitivity to CB-839 or glutamine withdrawal. This lower sensitivity may be due to the fact that KEAP1 mutations may not be biallelic, or H1355 cell line may harbor additional mutations, which could imbalance redox homeostasis and therefore affect sensitivity to glutaminase inhibition.

We next analyzed the proliferation rate of A549 (glutaminase inhibitor–sensitive) cells in glucose- or glutamine-free medium, and we found that glucose deprivation impaired growth by approximately 60%, whereas glutamine deprivation decreased proliferation by 90% (Fig. 3C). Likewise, glutamine deprivation
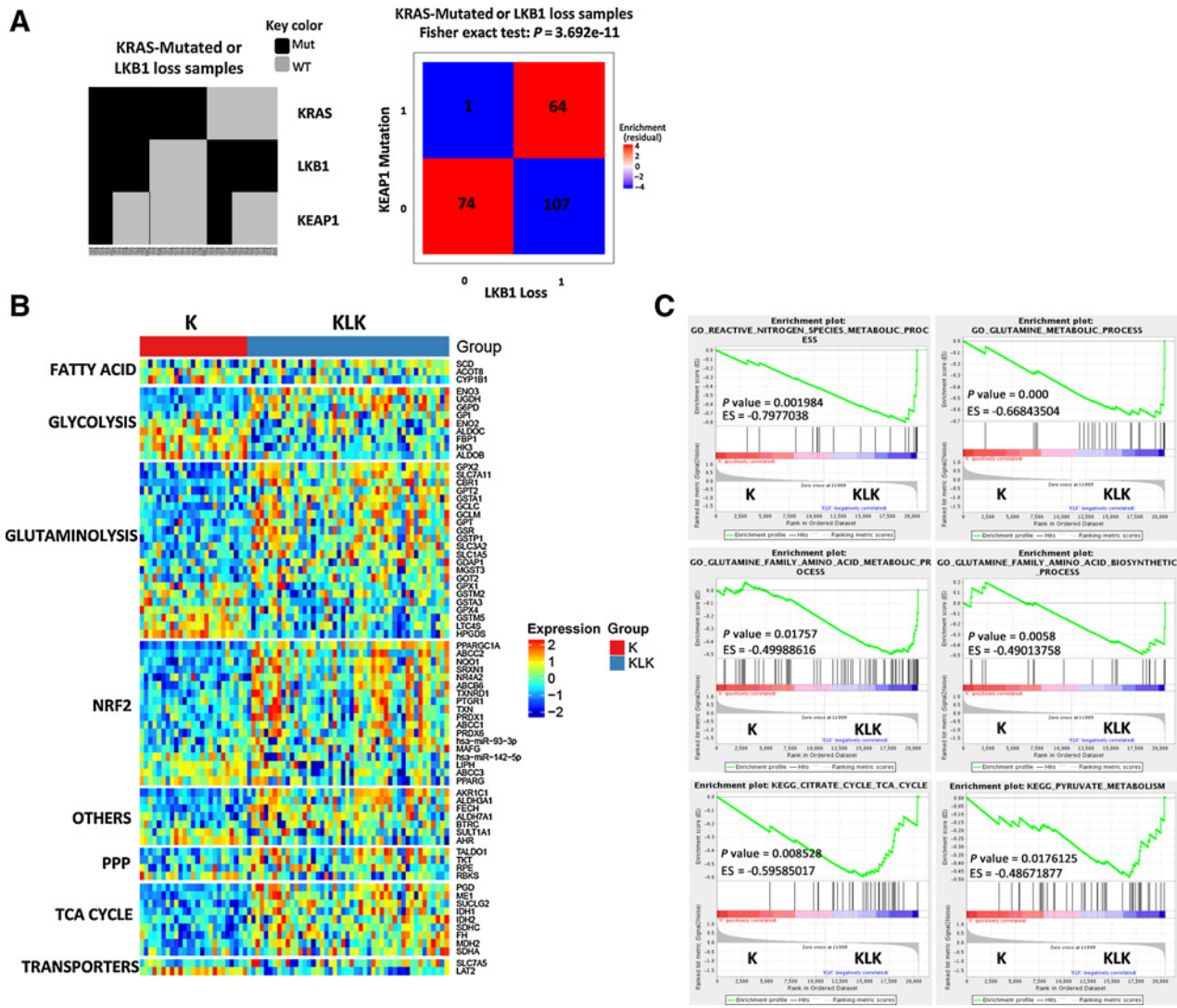
Figure 1.

KRAS-mutant tumors with functional inactivation of *STK11*/LKB1 and a KEAP1 comutation (KLK tumors) exhibit evidence of metabolic reprograming and adaptation to oxidative and energetic stress. **A,** Comutation plot for 246, predominantly early-stage, *KRAS*-mutant lung adenocarcinomas from the TCGA dataset. **B,** Heatmap depicting mRNA expression levels of significantly associated genes selected for the indicated pathways. **C,** GSEA shows significant enrichment of gene expression signatures in KLK subset compared with K subset.

(compared with complete medium) increased tumor cell apoptosis induction after treatment with H_2O_2 (Fig. 3D). Furthermore, glutamine withdrawal sensitivity and glutamate secretion both displayed a positive correlation with glutaminase sensitivity (Fig. 3E).

Glutaminase is the rate-limiting enzyme that converts glutamine to glutamate, the precursor for GSH synthesis, and glutaminase is critical for regulating redox balance (Fig. 3A). We analyzed the effect of pharmacologic glutaminase inhibition with CB-839. Treatment with 1 μmol/L CB-839 completely inhibited colony formation in A549 cells and H2030 cells (Supplementary Fig. S4A) and cellular proliferation (Fig. 3F; Supplementary Fig. S4B). Similarly, glutaminase inhibition induced cell-cycle arrest at the G_0–G_1 phase (Fig. 3G). Furthermore, treatment with CB-839 significantly increased ROS levels after 24 and 72 hours of incubation of glutaminase inhibition

(Fig. 4A). Glutaminase inhibition also significantly decreased cellular levels of ATP and GSH and reduced the NADPH/NADP$^+$ ratio (Fig. 4B–D). Although glutaminase inhibition alone did not induce cell death in A549 cells, CB-839 significantly increased the sensitivity of A549 cells to ROS stress (Fig. 4E). While ROS levels were increased by CB-839, treatment with a ROS scavenger NAC (N-acetyl-l-cysteine) significantly reduced intracellular ROS levels (Fig. 4F). However, treatment with NAC or with L-glutamate only partially abrogated the effect of CB-839 on cell proliferation (Fig. 4G and H; Supplementary Fig. S5A) and cell viability (Supplementary Fig. S5B and S5C) and likewise rescued the cell cycle from glutaminase inhibitor–induced cell-cycle arrest (Fig. 4I). These findings indicate that in these cells, glutamine metabolism is critical for cell proliferation and ROS scavenging, providing tumor cells a mechanism to survive in a high-ROS environment.
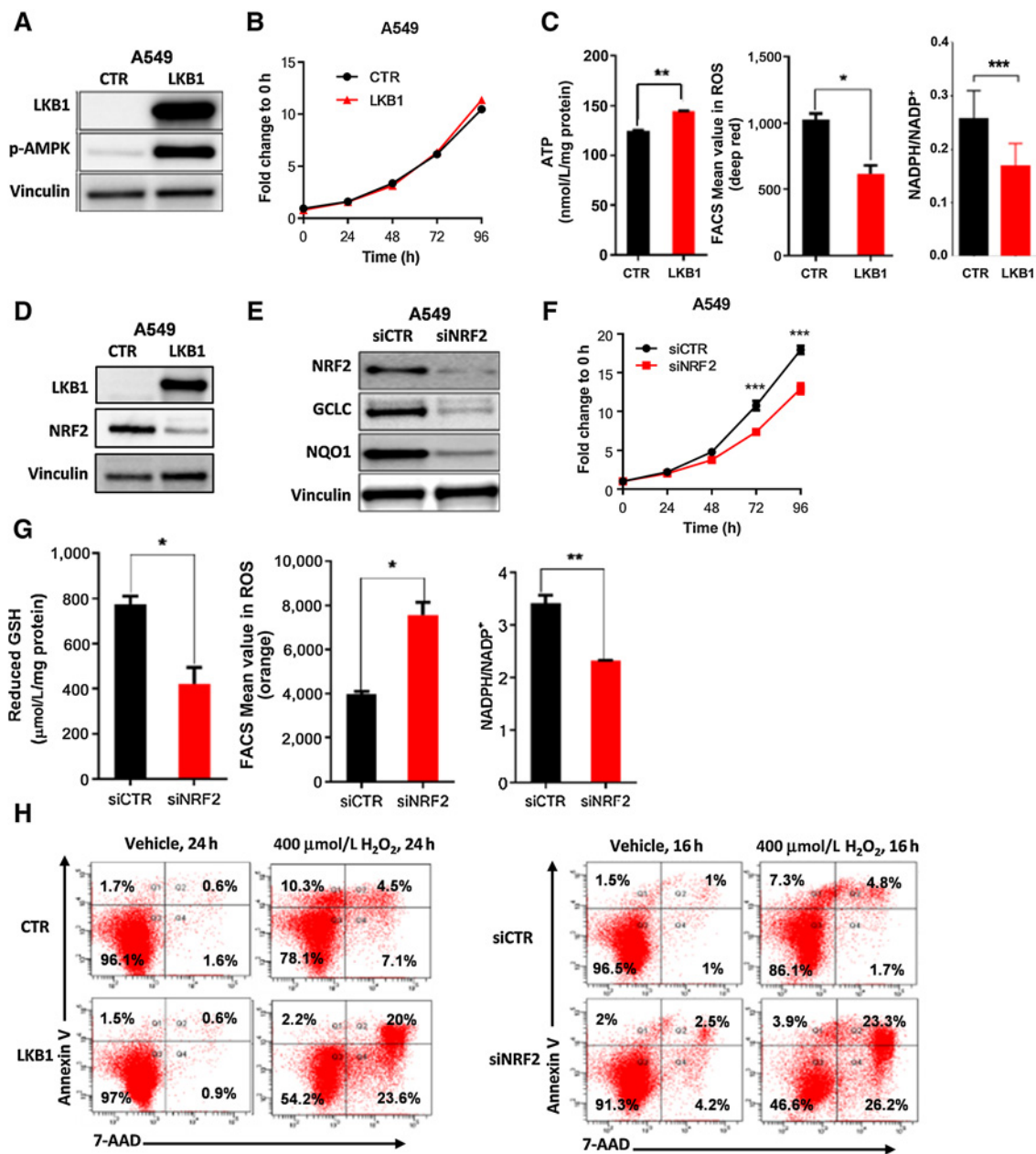
Figure 2.
The NRF2 pathway is modulated in *KRAS*-mutant LKB1-deficient tumors. **A,** Western blot analysis of stable expression of wild-type LKB1 in LKB1-deficient A549 cells and p-AMPK expression used as a functional control of LKB1 overexpression. Vinculin was used as a loading control. **B,** Cell proliferation assessed by the SRB assay in A549 cells with LKB1 overexpression, compared with empty vector control cells ($n = 5$; mean of three technical replicates from a representative experiment is shown in the graph). **C,** ATP measurement was analyzed using the ATPlite luminescence assay ($n = 1$), intracellular ROS levels were monitored using CellRox Deep Red and flow cytometry ($n = 3$; mean of two technical replicates from a representative experiment is shown in the graph), and the relative NADPH/NADP$^+$ ratio was determined using the NADP/NADPH-Glo assay ($n = 1$) in A549 cells with LKB1 overexpression, compared with vector control cells. **D,** Western blot analysis showing that NRF2 protein expression was higher in LKB1-overexpressing clones than in vector control cells. **E,** NRF2 expression was knocked down by siRNA in A549 cells and Western blot analysis was used to determine expression levels of the NRF2 target genes *GCLC* and *NQO1*. **F,** Cell proliferation was assessed using the SRB assay in NRF2-knockdown A549 cells compared with vector control cells ($n = 6$; mean of five technical replicates from a representative experiment is shown in the graph). **G,** Intracellular GSH levels were analyzed using the GSH-Glo assay ($n = 2$; mean of two technical replicates from a representative experiment is shown in the graph), ROS levels were measured using CellRox Deep Red and flow cytometry ($n = 3$; mean of two technical replicates from a representative experiment is shown in the graph), and the relative NADPH/NADP$^+$ ratio was determined using the NADP/NADPH-Glo assay ($n = 1$; mean of two technical replicates from a representative experiment is shown in the graph) in NRF2-knockdown A549 cells, compared with vector control cells. **H,** Apoptosis in A549 cells at 24 hours and 16 hours after treatment with 400 µmol/L H$_2$O$_2$ in LKB1 overexpression clones and NRF2 knockdown clones compared with vector control cells, determined by PE-conjugated Annexin-V/7-AAD staining and flow cytometry ($n = 1$). All data are presented as mean ± SEM (error bars). Statistical significance: *, $P \leq 0.05$; **, $P \leq 0.01$; ***, $P \leq 0.001$.
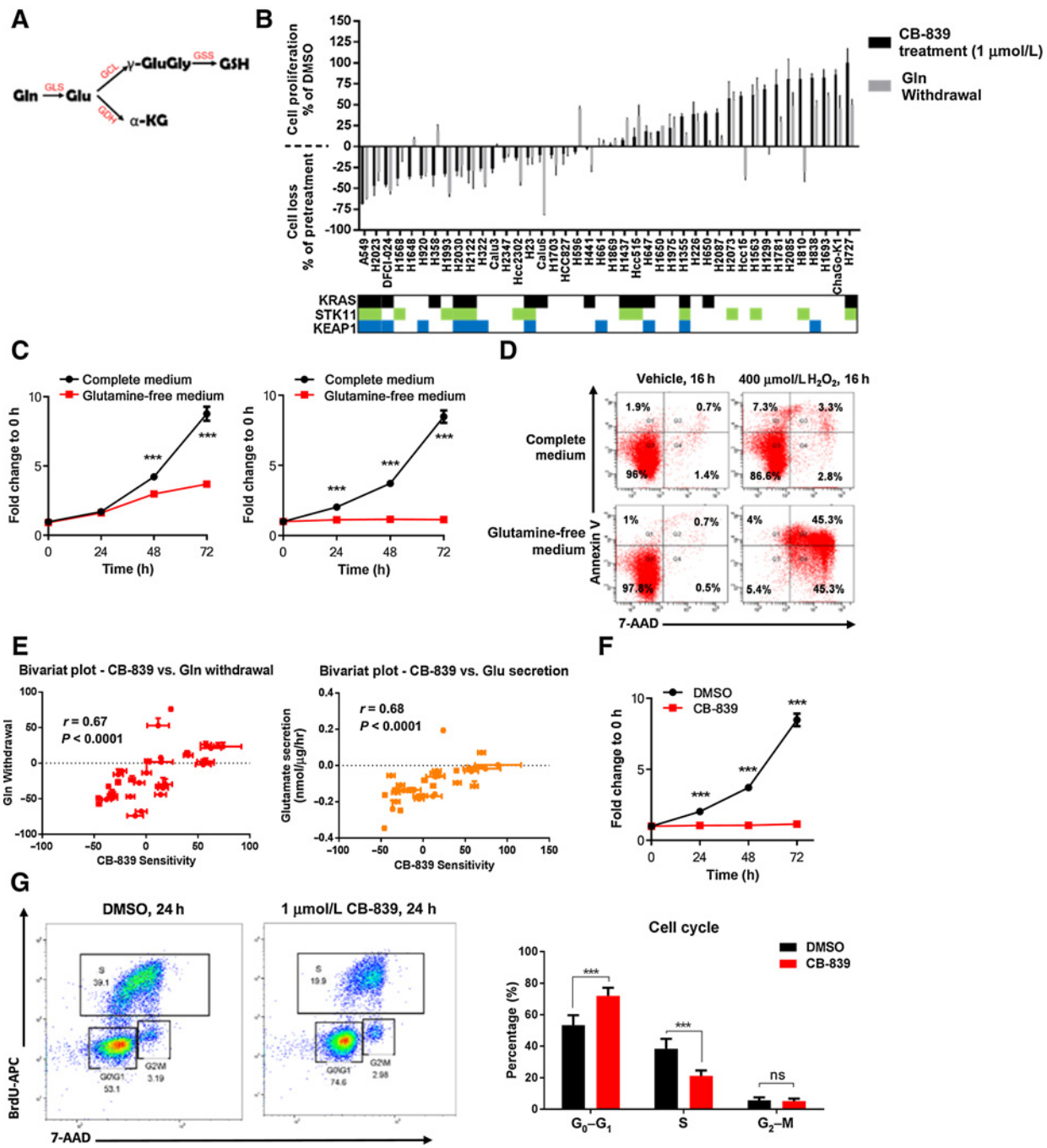
Figure 3.

Effects of glutaminase blocking in KL tumor cells line. **A,** Glutamine (Gln) is the precursor of glutathione (GSH). The first step is Gln conversion to glutamate (Glu) by glutaminase (GLS) glutamate dehydrogenase (GDH) converts Glu to α-ketoglutarate (α-KG), an important TCA cycle metabolite. Glu is catalyzed by two sequential enzymatic reactions. First, glutamine-cysteine ligase (GCL) catalyzes the formation of gamma-glutamylcysteine (γ-GluGly) from Glu and cysteine. Glutathione synthetase (GSS) then couples glycine to γ-GluGly to form GSH. **B,** Cell proliferation or loss measured in NSCLC cell lines after treatment with 1 μmol/L CB-839 for 72 hours. The mean and SEM of at least duplicate measurements are shown. **C,** Cell proliferation assessed by the SRB assay in A549 cells in complete, glucose-free, or glutamine-free medium ($n = 3$; mean of five technical replicates from a representative experiment is shown in the graph). **D,** Apoptosis, determined by PE-conjugated Annexin-V/7-AAD staining, in A549 cells at 16 hours after treatment with 0 or 400 μmol/L H_2O_2 in complete or glutamine-free medium ($n = 1$). **E,** Bivariant plots showing correlations between CB-839 sensitivity with glutamine withdrawal sensitivity or glutamate secretion. **F,** Cell proliferation, assessed by the SRB assay, in A549 cells after treatment with 1 μmol/L CB-839 ($n = 4$; mean of five technical replicates from a representative experiment is shown in the graph). **G,** Two-dimensional flow cytometry [propidium iodide + bromodeoxyuridine (BrdU)] after BrdU incorporation performed in A549 cells at 24 hours after treatment with 1 μmol/L CB-839 ($n = 1$). The percentage of cells in each phase of the cell cycle is provided ($n = 3$). All data are presented as mean ± SEM (error bars). Statistical significance: ***, $P \leq 0.001$. ns, nonsignificant.
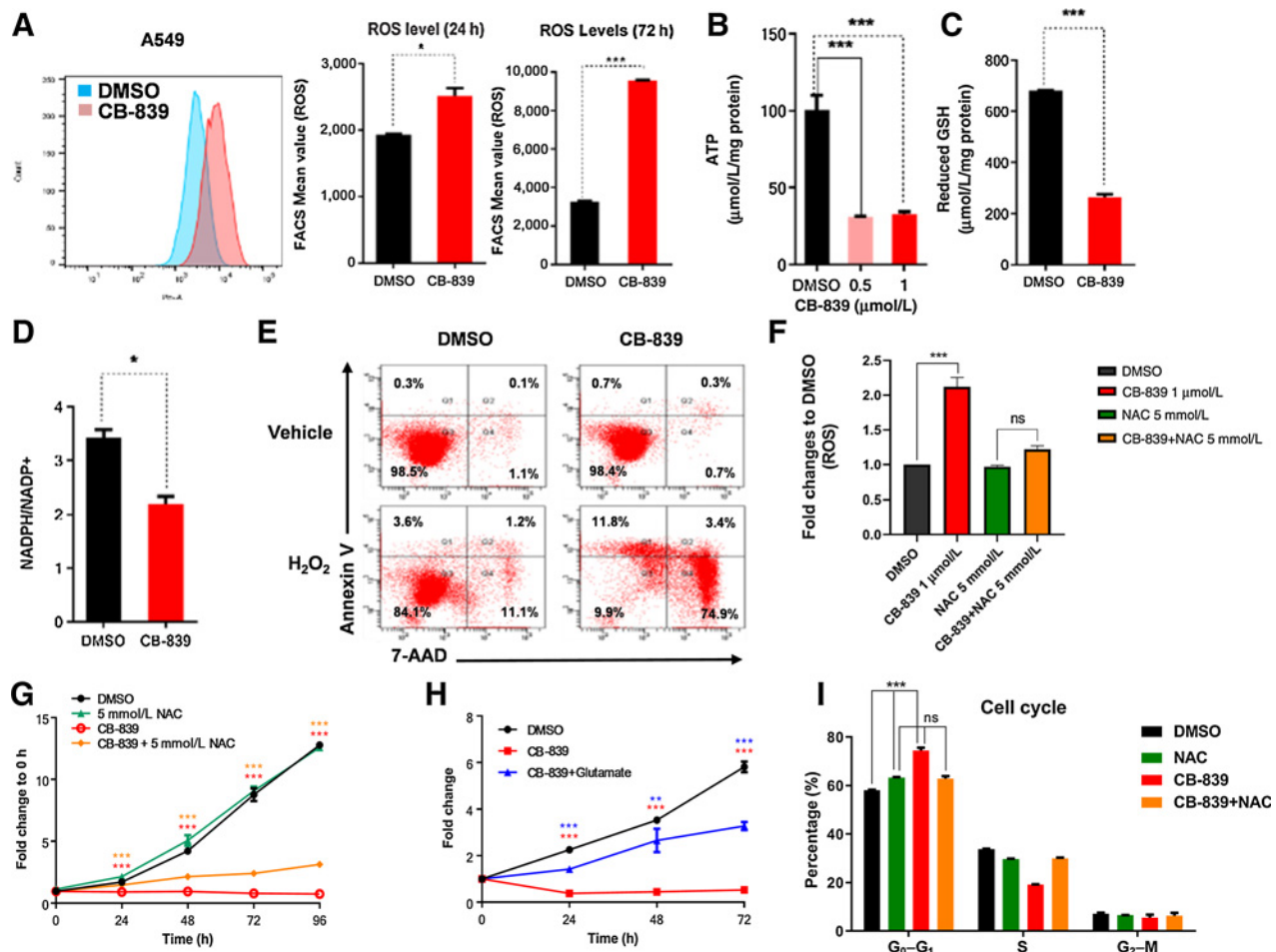
Figure 4.
Glutaminase inhibition increases energetic and oxidative stress sensitivity in *KRAS*-mutant LKB1-deficient tumors. **A,** Flow cytometry measurement of fluorescence intensity and bar graph of intracellular ROS in A549 cells at 24 and 72 hours after treatment with 1 μmol/L CB-839 ($n = 4$; mean of two technical replicates from a representative experiment are shown in the graph). **B,** ATP measurement, determined by the ATPlite luminescence assay, in A549 cells at 24 hours after treatment with 0.5 μmol/L and 1 μmol/L CB-839 ($n = 3$; mean of three technical replicates from a representative experiment are shown in the graph). **C** and **D,** Intracellular glutathione (GSH) levels analyzed by the GSH-Glo assay (**C**) and relative NADPH/NADP$^+$ ratio analyzed by the NADP/NADPH-Glo assay ($n = 2$ technical replicates/data point; **D**) in A549 cells at 24 hours after treatment with 1 μmol/L CB-839 ($n = 2$ technical replicates/data point). **E,** Apoptosis in A549 cells at 16 hours after treatment with 1 μmol/L CB-839 in the presence or absence of 200 μmol/L H$_2$O$_2$, determined by PE-conjugated Annexin-V/7-AAD staining ($n = 1$). **F,** Flow cytometry fluorescence intensity of intracellular ROS in A549 cells at 48 hours after treatment with 1 μmol/L CB-839 ($n = 3$; mean of three independent experiments are shown in the graph). **G,** Cell growth curve in A549 cells after treatment with 1 μmol/L CB-839 plus 5 mmol/L NAC ($n = 5$ technical replicates/data point). **H,** Cell growth curve in A549 cells after treatment with 1 μmol/L CB-839 plus 2 mg/mL L-glutamate ($n = 3$; mean of five technical replicates from a representative experiment are shown in the graph). **I,** Cell-cycle analysis of A549 cells at 24 hours after treatment with 5 mmol/L NAC, 1 μmol/L CB-839, and 1 μmol/L CB-839 combined with 5 mmol/L NAC ($n = 2$ technical replicates/data point). The percentage of cells in each phase of the cell cycle is provided. All data are presented as mean ± SEM (error bars). Statistical significance: *, $P \leq 0.05$; ***, $P \leq 0.001$. ns, nonsignificant.

LKB1 and KEAP1/NRF2 signaling pathways cooperatively contribute to glutaminase inhibitor sensitivity

As described previously, KL NSCLC cells typically exhibit upregulation of the NRF2/KEAP1 pathway, which may be a compensatory mechanism to maintain redox homeostasis, in part, through the NRF2-regulated antioxidant genes such as *GCLC*. To determine whether LKB1 loss and/or KEAP1/NRF2 pathway activation are direct contributors to glutaminase inhibitor sensitivity, we studied isogenic pairs of A549 cell lines with or without stable expression of wild-type LKB1 and/or siRNA-mediated NRF2 downregulation (Fig. 5A). LKB1 overexpression or NRF2 knockdown individually significantly decreased glutaminase inhibitor

sensitivity (Fig. 5B and C; Supplementary Fig. S6A). The combination of both modifications further reduced sensitivity to glutaminase inhibition to a greater extent than either alteration alone, rendering the cells essentially completely resistant to this treatment. ROS levels after treatment with CB-839 were also quantified, showing the same trend (Fig. 5D). Moreover, although glutaminase inhibition increased ROS production in A549 cells and A549/siNRF2 cells, ROS levels were not considerably altered by glutaminase inhibition in A549/LKB1 and A549/LKB1+siNRF2 cells (Fig. 5D). Also, although glutaminase inhibition decreased ATP levels in A549 cells as well as in A549/siNRF2 and A549/LKB1 cells, glutaminase inhibition had
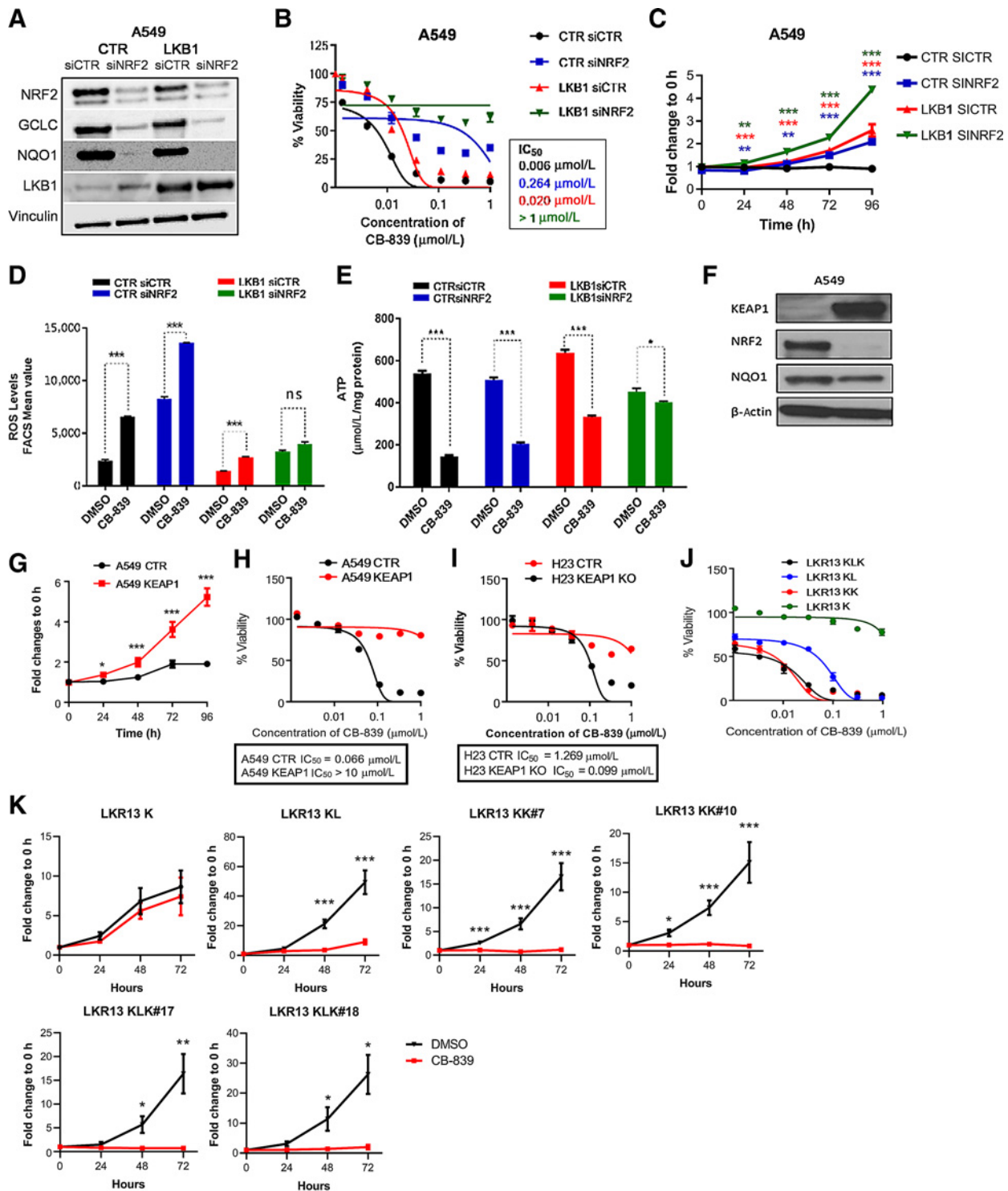
Figure 5.
LKB1 and KEAP1/NRF2 signaling pathways cooperatively contribute to glutaminase inhibition sensitivity. **A,** Western blot analysis of stable expression of wild-type LKB1 in A549 cells and NRF2 knockdown by siRNA (siNRF2). NRF2 gene targets *GCLC* and *NQO1* were used as a control. Vinculin was used as a loading control. **B,** Dose–response curves of cell viability by CellTiter-Glo of isogenic LKB1 pairs of A549 cells with or without NRF2 knockdown treated with CB-839 for 72 hours ($n = 5$; mean of three technical replicates from a representative experiment are shown in the graph). **C,** Cell proliferation assessed by the SRB assay in isogenic LKB1 pairs of A549 cells with or without NRF2 knockdown after treatment with 1 μmol/L CB-839 ($n = 2$; mean of five technical replicates from a representative experiment are shown in the graph). (*Continued on the following page.*)

minimal effect on A549/LKB1+siNRF2 cells (Fig. 5E). Similarly, KEAP1 overexpression in A549 cells decreased expression of NRF2 (Fig. 5F) and reduced sensitivity to CB-839 (Fig. 5G and H). Consequently, knockdown of KEAP1 in H23 cells increased the growth inhibition induced by glutaminase inhibition (Fig. 5I). Overexpression of LKB1 in A549 and H460 isogenic pairs also increased cell viability after 96 hours of treatment with CB-839 (Supplementary Fig. S6B).

Parallel experiments were performed using additional murine isogenic cell lines with or without LKB1 and KEAP1. KRAS-mutant primary cell line (LKR13 K) was established from an adenocarcinoma derived from Kras[LA1] mice. Isogenic pairs were generated by knocking out STK11 and KEAP1 genes using the CRISPR/Cas9 system. Consistent with the findings in human NSCLC cell lines, cells with both LKB1 and KEAP loss (LKR13 KLK) were the most sensitive to glutaminase inhibition. Loss of the individual genes KEAP1 (LKR13 KK) or LKB1 (LKR13 KL) enhanced sensitivity to glutaminase inhibition to a lesser extent, and IC_{50} was higher compared with LKR13 KLK. In contrast, KRAS cells with neither LKB1 nor KEAP1 loss (LKR13 K) displayed a clear resistance to CB-839 (Fig. 5J and K; Supplementary Fig. S6C). Intracellular ROS levels were also analyzed in LKR13 cells with or without LKB1 or KEAP1 following treatment with CB-839. We observed that the individual loss of LKB1 or KEAP1 resulted in enhanced sensitivity to CB-839 in terms of redox induction (Supplementary Fig. S6D). Taken together, these data provide a strong evidence that the LKB1 and KEAP1/NRF2 pathway cooperatively impact glutaminase inhibitor sensitivity.

To investigate the in vivo activity of glutaminase inhibition, we subcutaneously implanted tumors derived from KLK and KP (KRAS plus TP53 mutations) patients into female BALB/c nude mice. Once tumors reached 100 mm^3, animals were randomized into treatment groups. The glutaminase inhibitor significantly impaired tumor growth in KLK tumors (Fig. 6A); mice treated with CB-839 had significantly smaller tumors than mice in the vehicle group after 14 days of treatment ($P \leq 0.05$). Glutaminase inhibition did not significantly affect the growth of KP tumors (Fig. 6B), supporting a role for LKB1 and KEAP1 pathways in glutaminase inhibitor sensitivity. In addition, we subcutaneously implanted A549 (KLK) and isogenic A549 cells with KEAP1 expression (A549-KEAP1, KL) cells into female BALB/c nude mice and tested the effects of glutaminase inhibition on tumor growth. The glutaminase inhibitor, CB-839, impaired tumor growth in A549 (KLK) tumors (Fig. 6C; $P \leq$ 0.05 vs. vehicle-treated mice). However, glutaminase inhibition did not significantly affect the growth of A549/KEAP1 (KL) tumors (Fig. 6D).

LKB1 and KEAP1/NRF2 signaling pathways drive metabolic reprogramming in KLK tumor cells

We hypothesized that LKB1 and KEAP1 comutations could be contributing to glutaminase inhibitor sensitivity by driving glutamine-dependent metabolism. To test this hypothesis, we further evaluated the impact of the LKB1 and KEAP1/NRF2 pathways on glutamine metabolism. We analyzed cell proliferation rates in isogenic A549 cells with or without LKB1 or NRF2 expression with decreasing concentrations of glutamine in the culture medium. For all cells, growth rates were unchanged in medium containing low concentrations of glutamine (0.5 mmol/L) compared with normal medium. However, when cells were cultured in glutamine-free medium, only LKB1/siNRF2 A549 cells were able to proliferate at a rate similar to that of cells grown in normal medium (Fig. 7A). The growth of A549/siNRF2 cells was partially impaired in glutamine-free medium, and the proliferation of A549 control and A549/LKB1 cells was completely inhibited in glutamine-free conditions (Fig. 7A). Likewise, glucose-free medium did not affect cellular proliferation in A549/LKB1+siNRF2 cells, although it only partially impaired cell growth in A549 control cells (Supplementary Fig. S7A). These data indicate that cells with intact LKB1 and KEAP1/NRF2 pathways are able to grow with either glucose or glutamine, while cells with inactivation of both pathways are strongly dependent on glutamine.

Next, to test whether LKB1 and/or KEAP1/NRF2 pathways are responsible for metabolic reprogramming with a shift in glutamine utilization, we evaluated cellular accumulation of glutamine. We measured levels of cellular glutamine in cells grow in normal culture medium, and we observed nearly three times greater intracellular accumulation of glutamine in A549/LKB1+siNRF2 cells compared with A549 control cells (Fig. 7B). Glucose uptake after blocking of KEAP1/NRF2 pathway was also evaluated, showing higher rates in both A549/KEAP1 and A549/siNRF2 cells compared with A549 control cells. Furthermore, inhibition of glutamine metabolism by glutaminase inhibitor showed a similar effect in A549 control cells. Likewise, increment of glucose uptake rates after glutaminase inhibition was lower in A549/KEAP1 cells than in A549 control cells (Supplementary Fig. S7B). These results indicate that KLK cells use mainly glutamine to support metabolism, while cells with a functional KEAP1/NRF2 pathway have relatively greater glucose consumption.

Because NRF2 has been reported to activate genes involved in PPP and purine nucleotide production (22), and glutamine is needed in this process, we treated cells with exogenous nucleotides to determine whether they could compensate for the effects of glutaminase inhibition. Only adenine was able to partially rescue A549 (Fig. 7C) and H2030 cells (Supplementary Fig. S7D)

(Continued.) **D,** Flow cytometry measurement of the fluorescence intensity of intracellular ROS in isogenic LKB1 pairs of A549 cells with or without NRF2 knockdown at 24 hours after treatment with 1 µmol/L CB-839 ($n = 2$ technical replicates/data point). **E,** ATP measurement, according to the ATPlite luminescence assay, in isogenic LKB1 pairs of A549 cells with or without NRF2 knockdown at 24 hours after treatment with 1 µmol/L CB-839 ($n = 3$ technical replicates/data point) **F,** Western blot analysis showing KEAP1 overexpression in stable clones generated in A549 cells. **G,** Cell proliferation, assessed by the SRB assay, in isogenic KEAP1 pairs of A549 cells after treatment with 1 µmol/L CB-839 ($n = 2$; mean of five technical replicates from a representative experiment are shown in the graph). **H,** Dose–response curves of cell viability of isogenic KEAP1 pairs in A549 cells treated with CB-839 ($n = 3$; mean of three technical replicates from a representative experiment are shown in the graph). **I,** Dose–response curve by CellTiter-Glo of H23 control and KEAP1 knockout (KO) cells after treatment with 1 µmol/L CB-839 ($n = 3$; mean of three technical replicates from a representative experiment are shown in the graph) for 72 hours. **J,** Dose–response curve by CellTiter-Glo of LKR13 K, KL, KLK, and KK cells after treatment with 1 µmol/L CB-839 ($n = 3$; mean of three technical replicates from a representative experiment are shown in the graph) for 72 hours. **K,** Cell proliferation assessed by cell counting method in isogenic pairs of LKR13 KRAS mutant (K), with LKB1 knockout (KL), KEAP1 knockout (KK), or both together (KLK) after treatment with 1 µmol/L CB-839 ($n = 3$–4; mean of 3–4 independent experiments are shown in the graph). All data are presented as mean ± SEM (error bars). Statistical significance: *, $P \leq 0.05$; **, $P \leq 0.01$; ***, $P \leq 0.001$.
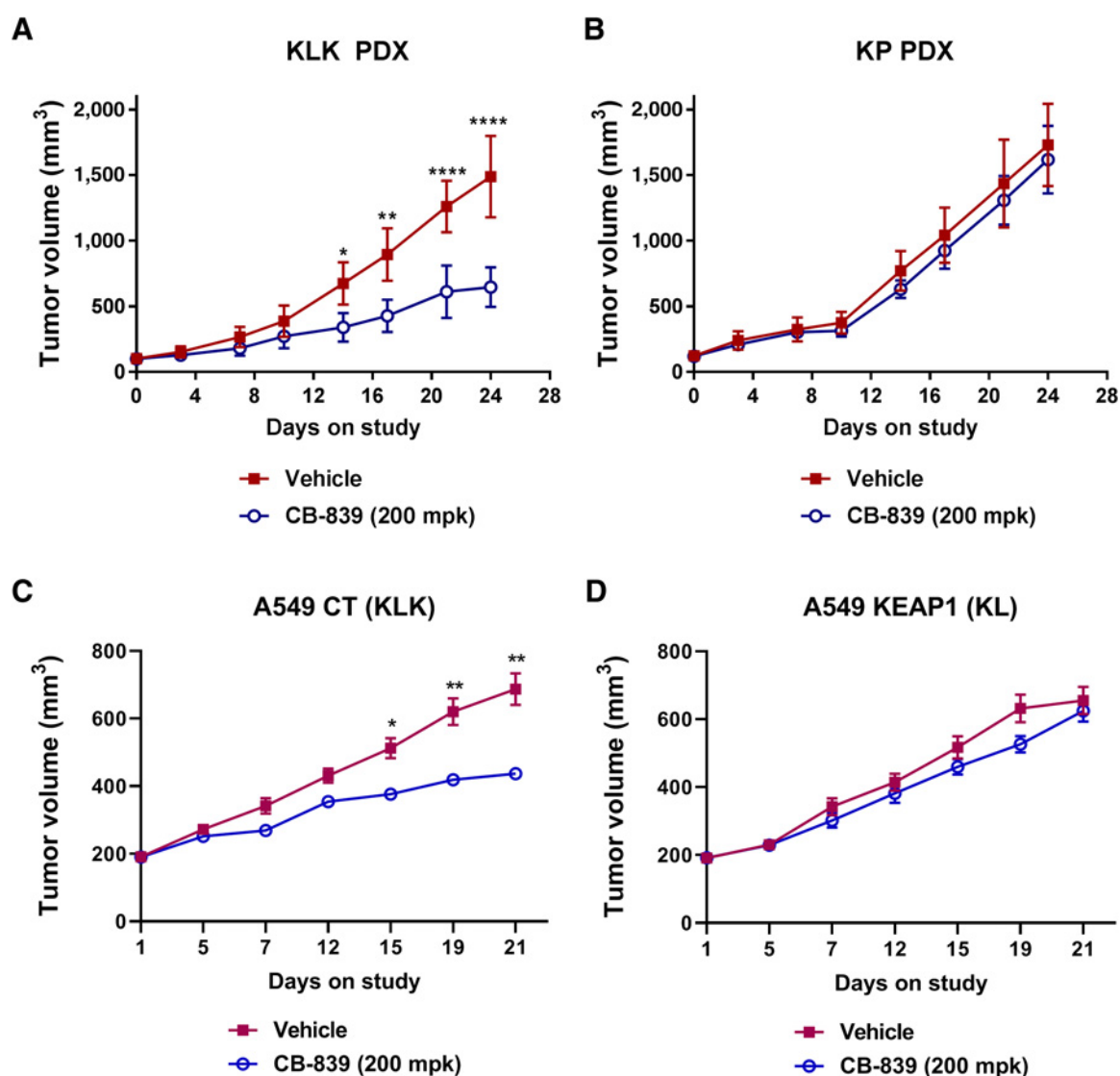
Figure 6.
Glutaminase inhibitors selectively impair tumor growth *in vivo* in KLK tumors. Tumor volume measured in PDX derived from KLK (**A**) and KP (**B**) tumors, A549 CT (KLK; **C**), and A549 KEAP1 (KL; **D**) in nude mice, dosed orally with CB-839 (200 mg/kg) or vehicle (ß-cyclodextrin pH 2) twice daily for 28 or 21 days. All data are presented as mean ± SEM (error bars) for each group (n = 8). Statistical significance: *, $P \leq 0.05$; **, $P \leq 0.01$; ***, $P \leq 0.001$; ****, $P < 0.0001$.

following treatment with CB-839. Furthermore, in cells with high expression of NRF2, glucose is preferentially metabolized through the PPP, limiting the contribution of this carbon fuel to glycolysis and TCA intermediates. Consequently, the antitumor cell activity of CB-839 was abrogated by the addition of the glycolytic intermediate pyruvate. Similarly, the addition of α-ketoglutarate rescued H2030 cells but not A549 cells (Fig. 7D; Supplementary Fig. S7C), suggesting that glutamine and glutaminolysis are the main source of anaplerosis in KLK tumors. Consistent with this finding, the addition of pyruvate rescued the cell-cycle arrest after glutaminase inhibition (Supplementary Fig. S7F).

Because cells can also grow through the hexosamine pathway, which is supported by glucose or glutamine, we analyzed the effect of the addition of hexosamine intermediates (glucosamine-6-P and N-acetylglucosamine-1-P) on cells treated with glutaminase inhibitor. None of hexosamine pathway intermediates could completely reverse the effects of glutaminase inhibition on cell viability (Supplementary Fig. S7E), indicating that the effect of CB-839 was not mediated by the hexosamine pathway. Glutamine can also serve as nitrogen source for amino acid and protein synthesis, thus we next evaluated the impact of the addition of different amino acids to cells treated with glutaminase inhibitor. Only the addition of L-glutamate, an intermediate of glutaminolysis, abrogated the effects of CB-839 on cell proliferation and viability (Fig. 7F and G), suggesting that glutaminase inhibitor is not affecting amino acid synthesis.

To further investigate the role of glutamine in the TCA cycle in KLK cells, a metabolic profile analysis was performed using A549

cells (glutaminase inhibitor–sensitive) and H727 (glutaminase inhibitor–resistant) cells following glutaminase inhibition (Fig. 7H). TCA intermediate levels were reduced in both cell lines compared with nontreated cells, but these levels were significantly lower in the A549 cells, indicating that glutaminase inhibition impairs the TCA cycle particularly in the A549 cells with both LKB1 and KEAP1 deficiency. These data confirm that beyond ROS homeostasis, glutaminase inhibition has a direct impact on cellular metabolism by affecting the progression of the TCA cycle.

Collectively, these results suggest that in KLK tumor cells, activation of the KEAP1/NRF2 pathway limits metabolic flexibility and promotes glutamine-addictive metabolism to maintain TCA cycle in addition to redox homeostasis, rendering these tumor cells selectively vulnerable to glutaminase inhibitors.

Discussion

NSCLC remains the leading cause of cancer-related mortality worldwide despite substantial therapeutic advances. *STK11* (LKB1) is the second most commonly altered tumor suppressor in NSCLC and often cooccurs with *KRAS* mutations (K). However, there are currently no approved treatment strategies tailored for *KRAS*-mutant or LKB1-deficient (KL) NSCLC. Here, we report that the altered metabolism within KL tumors enhances redox and energetic stress, which is compensated by the cooccurring loss of KEAP1. Furthermore, LKB1 loss and KEAP1/NRF2 (KLK) pathway activation cooperatively drive a glutamine-addicted metabolic program for maintenance of redox homeostasis in the face of these increased stresses, rendering KLK cells more sensitive to glutaminase inhibition. Collectively, our data indicate that deregulation of the LKB1 and KEAP1/NRF2 pathways together is responsible for this vulnerability, and glutaminase inhibition may be a promising treatment strategy for KLK NSCLC.

The LKB1–AMPK axis is a primary energetic sensor maintaining intracellular ATP and NADPH levels in conditions of metabolic stress (6, 7). Through activation of the mTOR pathway, the LKB1–AMPK axis modulates cell proliferation (8). Therefore, LKB1-deficient tumors are characterized by uncontrolled cellular proliferation with elevated energetic stress, which increases intracellular ROS concentrations. LKB1 has also been shown to function as a negative regulator of cellular ROS stress (9, 23, 24). Several studies have reported high levels of the antioxidant NRF2 in lung cancer, among other cancers; NRF2 not only enhances cell proliferation and promotes therapeutic resistance owing to its antioxidant property (25–32), but also drives a metabolic and biochemical rewiring (18, 33) that may provide specific vulnerabilities (34). Likewise, we observed that KL tumors may be particularly resistant to the high ROS accumulation within the tumor microenvironment, through an enrichment of *KEAP1*-inactivating mutations and enhanced expression of NRF2-regulated genes (4). Our findings indicate that while KL tumor cells exhibit increased energetic and ROS stress, LKB1-deficient cells with cooccurring *KEAP1*-inactivating mutations have developed an effective strategy to compensate for the ROS imbalance by using NRF2 to drive an antioxidant response in a glutamine-dependent manner. Interestingly, we also found that expression of LKB1 modulated NRF2 levels even when *KEAP1* is mutated, suggesting that the KEAP1/NRF2 pathway may be upregulated in KL tumors not only by *KEAP1* mutations, but also by increased

ROS induced by LKB1 loss. Although KEAP1 is the most important regulator of NRF2, there are likely alternative mechanisms that may contribute to the modulation of NRF2 activity by LKB1 (35). These results confirm that the KEAP1/NRF2 pathway plays a critical role in maintaining redox homeostasis in KL tumors. Activation of this compensatory network yields an aggressive cancer phenotype capable of proliferation and survival in a hostile tumor environment.

Glutamine metabolism alleviates oxidative stress by producing reduced GSH. Because KLK tumors exhibit enhanced activation of the NRF2 pathway, which regulates glutamine-mediated ROS detoxification (36), we used an orally bioavailable inhibitor of glutaminase, CB-839. This agent selectively and irreversibly inhibits glutaminase and has been reported to have antiproliferative effects in various tumor cell types (11–14, 16–18, 37, 38). Our findings demonstrate that glutaminase inhibition completely blocks cell proliferation in KLK NSCLC cells, in part, by increasing ROS and energetic stress. Interestingly, only LKB1-deficient cells harboring KEAP1/NRF2 pathway inactivation were fully sensitive to glutaminase inhibition, suggesting that LKB1 deficiency together with the KEAP1/NRF2 axis provides a specific vulnerability to blockade of glutamine metabolism.

Tumor cells exhibit a high demand for nutrients to maintain the elevated rate of proliferation. Therefore, the modification of normal metabolism is an important strategy for tumor cells to support their deregulated growth and survival. Although most cancers depend on a high rate of aerobic glycolysis for their growth, some cancer cells also display an addiction to glutamine, even though glutamine is a nonessential amino acid that can be synthesized from glucose (39, 40). *KRAS*-mutant tumors demonstrate metabolic reprogramming that enhances glutaminolysis (41–45). Consistent with our observations, the loss of LKB1 in NSCLC cells has also been shown to promote enhanced glucose and glutamine metabolism through increased expression of HIF-1α (46) and decreased metabolic flexibility, rendering LKB1-deficient tumor cells more sensitive to glutaminase inhibition (47). Furthermore, a recent publication indicated that KL squamous cell carcinoma (SCC) cells are more glycolytic-dependent compared with KL ADC, suggesting that ADC may be significantly less reliant on glucose metabolism, even when LKB1 is lost (48). Interestingly, KL SCC tumors became resistant to mTOR inhibition by upregulating glutamine metabolism, and mTOR inhibition in combination with CB-839 was able to overcome resistance (37, 49). On the other hand, NRF2 regulates genes encoding PPP enzymes and glutaminolysis-related proteins (36) and has been found to contribute to cancer development by modulating metabolism in addition to enhancing the cellular stress response (22). Supporting our data, KEAP1 loss has been shown to drive glutamine dependency and sensitivity to glutaminase inhibition in lung KP model (18, 33).

Our results indicate that KLK tumor cells exhibit reduced glucose metabolism efficiency, suggesting that LKB1 loss along with KEAP1 inactivation is responsible for shifting the cellular metabolism to become less glucose- and more glutamine-dependent. On the other hand, activation of NRF2 pathway has been shown to increase glucose uptake, which is preferentially metabolized through PPP to modulate antioxidant response (50, 51). Although it is not the main focus of this study, we also observed augmented glucose uptake with glutaminase inhibition
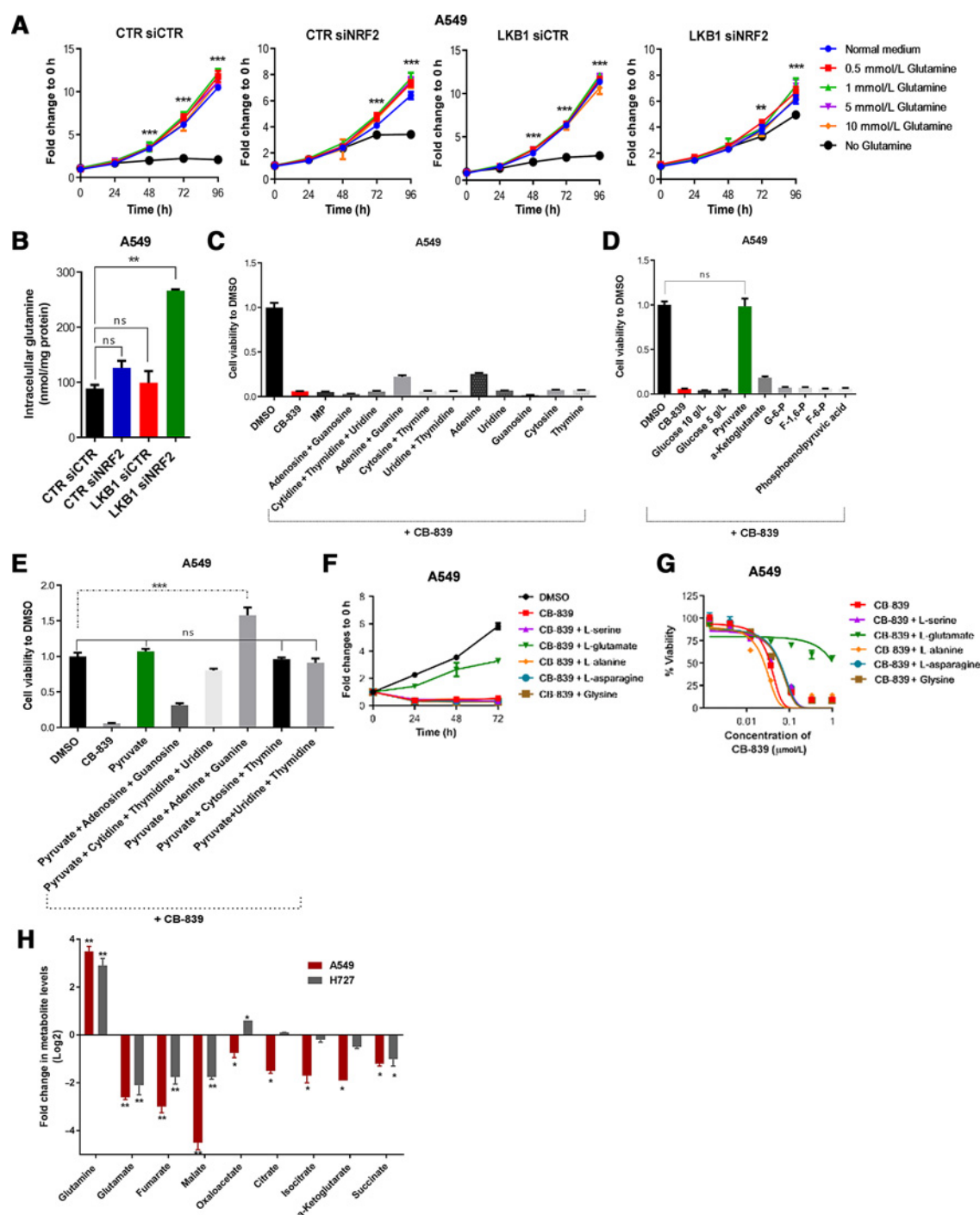
Figure 7.
Glutamate and pyruvate rescue cells treated with glutaminase inhibitors. **A,** Cell proliferation, assessed using the SRB assay, in isogenic LKB1 pairs of A549 cells with or without NRF2 knockdown, with different concentrations of glutamine ($n = 5$ technical replicates/data point). **B,** Intracellular concentrations of glutamine at 24 hours after treatment of isogenic LKB1 pairs of A549 cells with or without NRF2 knockdown ($n = 5$ technical replicates/data point). Cell viability of A549 cells treated with 1 μmol/L CB-839 and 100 μmol/L of exogenous nucleotides (**C**) and glycolysis and tricarboxylic acid intermediates (**D**) for 72 hours, as well as nucleotides plus glycolysis intermediates ($n = 3$ technical replicates/data point; **E**). **F,** Cell proliferation, assessed using the SRB assay, in A549 cells after treatment with 1 μmol/L CB-839 and the indicated concentrations of amino acids ($n = 2$; mean of five technical replicates from a representative experiment are shown in the graph. **G,** Dose–response curves of cell viability of A549 cells treated with the indicated concentrations of amino acids in the presence of different concentrations of CB-839 for 72 hours ($n = 3$; mean of five technical replicates from a representative experiment are shown in the graph). **H,** Quantification of TCA cycle intermediates in A549 (GLSi-sensitive) and A727 (GLSi-resistant) cells treated with 1 μmol/L of CB-839. All data are presented as mean $\pm$ SEM (error bars). Statistical significance: *, $P \leq 0.05$; **, $P \leq 0.01$; ***, $P \leq 0.001$. ns, nonsignificant.

suggesting it may compensate in the face of impaired glutamine utilization. This suggests that combination approaches targeting both glucose and glutamine utilization merit further investigation in these tumors.

Glutamine is essential for nucleotide biosynthesis because it donates nitrogen to purines and pyrimidines. Although glutaminase1 inhibition has been reported to affect pyrimidine synthesis, and LKB1 deficiency is associated with impaired purine and pyrimidine metabolism (52), the addition of thymidine or other pyrimidine nucleotides was not able to rescue KLK cells from glutaminase inhibition. However, the addition of the purine nucleotide adenine partially rescued KLK cells from glutaminase inhibition. Interestingly, NRF2 is required for an efficient purine nucleotide synthesis while at the same time promoting glutamine metabolism (22). Our results indicate that inhibition of glutamine metabolism may only partially limit purine nucleotide synthesis in KLK NSCLC cells, and therefore it is unlikely that the effect of glutaminase inhibition on proliferation was due, only, to impairment of DNA synthesis.

Glutamine metabolism also supports the production of α-ketoglutarate, as a carbon source, which enters into the TCA cycle. Tumors that are addicted to glutamine metabolism use it not only as an amino and amido source but also as a TCA anaplerotic source. The two major anaplerotic sources are glutamine and pyruvate, which depend on the enzymatic activity of glutaminase and pyruvate carboxylase (PC), respectively, to enter into the TCA cycle. Tumor cells have been reported to compensate for glutamine depletion by rerouting carbon from glucose and enhancing pyruvate carboxylase expression (53), and inhibition of import of mitochondrial pyruvate renders the glutaminolytic pathway essential for tumor cell survival (54). A gene signature predicting glutamine inhibition sensitivity has been recently established (55). Although KEAP1 loss was not identified as a predictive marker, the metabolic phenotype described for sensitive tumors was consistent with our finding in that study. Inhibition of glutaminase 1 significantly reduced amino acids, TCA and glutathione intermediates, and α-ketoglutarate and glutathione were able to rescue the cells from glutaminase inhibition, suggesting that resistant cells could be dependent on oxaloacetate and citrate as anapleorotic sources to maintain adaptive response despite to glutaminase inhibition (55). We observed similar results in our resistant model A427, where levels of both oxaloacetate and citrate were significantly higher after CB-839 treatment compared with sensitive A549 cells. Likewise, our data also indicate that the TCA cycle is blocked when glutamine metabolism is impaired in KLK tumor cells, and only pyruvate and α-ketoglutarate completely rescued cells from glutaminase inhibition. Previous studies have demonstrated that KEAP1 loss increases dependency on glutaminolysis and treatments with CB-839 directly affected the TCA cycle anaplerosis (18, 33). Collectively, our data indicate that glutaminase-resistant tumors are able to use different carbon sources to maintain TCA cycle precursors, while glutaminase-sensitive tumors are highly dependent on glutamine for TCA cycle maintenance. Thus, KLK tumor cells are highly dependent on glutamine metabolism, and both redox and bioenergetics stress drive sensitivity to glutaminase inhibition.

The data reported here provide a novel insight into the impact of LKB1 loss on tumor cell metabolism and the resulting selective vulnerabilities within this subset of NSCLC. Taken together, our findings show that LKB1 loss induces energetic and redox stress, which can be compensated for through activation of the KEAP1/NRF2 pathway, and that together these two pathways promote glutamine-addictive metabolism, rendering these tumor cells selectively sensitive to glutaminase inhibition. These findings have immediate clinical implications and support the future clinical testing of glutaminase inhibition in KLK NSCLC.

Disclosure of Potential Conflicts of Interest

F. Parlati has ownership interest (including stock and patents) in Calithera Biosciences. F. Skoulidis has received speakers bureau honoraria from Bristol-Myers Squibb. R.J. DeBerardinis is a consultant/advisory board member for Agios Pharmaceuticals. J.D. Minna has provided expert testimony for NIH Licencing Cell Lines and University of Texas Southwestern Medical Center Licencing Cell Lines. J.V. Heymach reports receiving commercial research grant from AstraZeneca, Bayer, GlaxoSmithKline, and Spectrum; has ownership interest (including stocks and patents) in Spectrum and Biotree; and is a consultant/advisory board member for AstraZeneca, Boehringer Ingelheim, Genentech, GSK, Guardant Health, Hengrui, Lilly, Novartis, and EMD Serono. No potential conflicts of interest were disclosed by the other authors.

Authors' Contributions

Conception and design: A. Galan-Cobo, J.V. Heymach
Development of methodology: A. Galan-Cobo, X. Qu, F. Skoulidis, J.V. Heymach
Acquisition of data (provided animals, acquired and managed patients, provided facilities, etc.): A. Galan-Cobo, P. Sitthideatphaiboon, X. Qu, A. Poteete, P.-H. Chen, L.K. Boroughs, M.L.M. Rodriguez, W. Zhang, F. Parlati, V. Gandhi, R.J. DeBerardinis, J.D. Minna
Analysis and interpretation of data (e.g., statistical analysis, biostatistics, computational analysis): A. Galan-Cobo, P. Sitthideatphaiboon, X. Qu, P. Tong, F. Parlati, J. Wang, F. Skoulidis, R.J. DeBerardinis, J.D. Minna
Writing, review, and/or revision of the manuscript: A. Galan-Cobo, P. Sitthideatphaiboon, X. Qu, F. Skoulidis, R.J. DeBerardinis, J.D. Minna, J.V. Heymach
Administrative, technical, or material support (i.e., reporting or organizing data, constructing databases): P. Sitthideatphaiboon, X. Qu, M.A. Pisegna
Study supervision: A. Galan-Cobo, J.V. Heymach
Others (grant support): J.D. Minna

Acknowledgments

References

1. Ihle NT, Byers LA, Kim ES, Saintigny P, Lee JJ, Blumenschein GR, et al. Effect of KRAS oncogene substitutions on protein behavior: implications for signaling and clinical outcome. J Natl Cancer Inst 2012;104:228–39.

2. Ding L, Getz G, Wheeler DA, Mardis ER, McLellan MD, Cibulskis K, et al. Somatic mutations affect key pathways in lung adenocarcinoma. Nature 2008;455:1069–75.

3. Weir BA, Woo MS, Getz G, Perner S, Ding L, Beroukhim R, et al. Characterizing the cancer genome in lung adenocarcinoma. Nature 2007;450: 893–8.

4. Skoulidis F, Byers LA, Diao L, Papadimitrakopoulou VA, Tong P, Izzo J, et al. Co-occurring genomic alterations define major subsets of KRAS-mutant lung adenocarcinoma with distinct biology, immune profiles, and therapeutic vulnerabilities. Cancer Discov 2015;5:860–77.

5. Ji H, Houghton AM, Mariani TJ, Perera S, Kim CB, Padera R, et al. K-ras activation generates an inflammatory response in lung tumors. Oncogene 2005;25:2105–12.

6. Shaw RJ, Kosmatka M, Bardeesy N, Hurley RL, Witters LA, DePinho RA, et al. The tumor suppressor LKB1 kinase directly activates AMP-activated kinase and regulates apoptosis in response to energy stress. Proc Natl Acad Sci U S A 2004;101:3329–35.

7. Jeon SM, Chandel NS, Hay N. AMPK regulates NADPH homeostasis to promote tumour cell survival during energy stress. Nature 2012;485: 661–5.

8. Lamming Dudley W, Sabatini David M. A central role for mTOR in lipid homeostasis. Cell Metab 2013;18:465–9.

9. Li F, Han X, Li F, Wang R, Wang H, Gao Y, et al. LKB1 inactivation elicits a redox imbalance to modulate non-small cell lung cancer plasticity and therapeutic response. Cancer Cell 2015;27:698–711.

10. Kansanen E, Kuosmanen SM, Leinonen H, Levonen AL. The Keap1-Nrf2 pathway: mechanisms of activation and dysregulation in cancer. Redox Biol 2013;1:45–9.

11. Chakrabarti G, Moore ZR, Luo X, Ilcheva M, Ali A, Padanad M, et al. Targeting glutamine metabolism sensitizes pancreatic cancer to PARP-driven metabolic catastrophe induced by ß-lapachone. Cancer Metab 2015;3:12.

12. Gross MI, Demo SD, Dennison JB, Chen L, Chernov-Rogan T, Goyal B, et al. Antitumor activity of the glutaminase inhibitor CB-839 in triple-negative breast cancer. Mol Cancer Ther 2014;13:890–901.

13. Guo L, Zhou B, Liu Z, Xu Y, Lu H, Xia M, et al. Blockage of glutaminolysis enhances the sensitivity of ovarian cancer cells to PI3K/mTOR inhibition involvement of STAT3 signaling. Tumor Biol 2016;37:11007–15.

14. Jacque N, Ronchetti AM, Larrue C, Meunier G, Birsen R, Willems L, et al. Targeting glutaminolysis has antileukemic activity in acute myeloid leukemia and synergizes with BCL-2 inhibition. Blood 2015;126:1346–56.

15. Katt WP, Cerione RA. Glutaminase regulation in cancer cells: a druggable chain of events. Drug Discov Today 2014;19:450–7.

16. Momcilovic M, Bailey ST, Lee JT, Fishbein MC, Magyar C, Braas D, et al. Targeted inhibition of EGFR and glutaminase induces metabolic crisis in EGFR mutant lung cancer. Cell Rep 2017;18:601–10.

17. Thompson RM, Dytfeld D, Reyes L, Robinson RM, Smith B, Manevich Y, et al. Glutaminase inhibitor CB-839 synergizes with carfilzomib in resistant multiple myeloma cells. Oncotarget 2017;8:35863–76.

18. Romero R, Sayin VI, Davidson SM, Bauer MR, Singh SX, LeBoeuf SE, et al. Keap1 loss promotes Kras-driven lung cancer and results in dependence on glutaminolysis. Nat Med 2017;23:1362.

19. Wislez M, Spencer ML, Izzo JG, Juroske DM, Balhara K, Cody DD, et al. Inhibition of mammalian target of rapamycin reverses alveolar epithelial neoplasia induced by oncogenic K-ras. Cancer Res 2005;65:3226–35.

20. Vichai V, Kirtikara K. Sulforhodamine B colorimetric assay for cytotoxicity screening. Nat Protoc 2006;1:1112–6.

21. Yuan M, Breitkopf SB, Yang X, Asara JM. A positive/negative ion–switching, targeted mass spectrometry–based metabolomics platform for bodily fluids, cells, and fresh and fixed tissue. Nat Protoc 2012;7:872.

22. Mitsuishi Y, Taguchi K, Kawatani Y, Shibata T, Nukiwa T, Aburatani H, et al. Nrf2 redirects glucose and glutamine into anabolic pathways in metabolic reprogramming. Cancer Cell 2012;22:66–79.

23. Whang YM, Park SI, Trenary IA, Egnatchik RA, Fessel JP, Kaufman JM, et al. LKB1 deficiency enhances sensitivity to energetic stress induced by erlotinib treatment in non-small-cell lung cancer (NSCLC) cells. Oncogene 2016;35: 856–66.

24. Xu HG, Zhai YX, Chen J, Lu Y, Wang JW, Quan CS, et al. LKB1 reduces ROS-mediated cell damage via activation of p38. Oncogene 2015;34:3848–59.

25. Jiang T, Chen N, Zhao F, Wang X-J, Kong B, Zheng W, et al. High levels of Nrf2 determine chemoresistance in type II endometrial cancer. Cancer Res 2010;70:5486–96.

26. Kim YR, Oh JE, Kim MS, Kang MR, Park SW, Han JY, et al. Oncogenic NRF2 mutations in squamous cell carcinomas of oesophagus and skin. J Pathol 2010;220:446–51.

27. Shibata T, Kokubu A, Gotoh M, Ojima H, Ohta T, Yamamoto M, et al. Genetic alteration of Keap1 confers constitutive Nrf2 activation and resistance to chemotherapy in gallbladder cancer. Gastroenterology 2008;135:1358–68.

28. Shibata T, Ohta T, Tong KI, Kokubu A, Odogawa R, Tsuta K, et al. Cancer related mutations in NRF2 impair its recognition by Keap1-Cul3 E3 ligase and promote malignancy. Proc Natl Acad Sci U S A 2008;105: 13568–73.

29. Singh A, Misra V, Thimmulappa RK, Lee H, Ames S, Hoque MO, et al. Dysfunctional KEAP1–NRF2 interaction in non-small-cell lung cancer. PLoS Med 2006;3:e420.

30. Solis LM, Behrens C, Dong W, Suraokar M, Ozburn NC, Moran CA, et al. Nrf2 and Keap1 abnormalities in non–small cell lung carcinoma and association with clinicopathologic features. Clin Cancer Res 2010;16: 3743–53.

31. Wang X-J, Sun Z, Villeneuve NF, Zhang S, Zhao F, Li Y, et al. Nrf2 enhances resistance of cancer cells to chemotherapeutic drugs, the dark side of Nrf2. Carcinogenesis 2008;29:1235–43.

32. Zhang P, Singh A, Yegnasubramanian S, Esopi D, Kombairaju P, Bodas M, et al. Loss of Kelch-like ECH-associated protein 1 function in prostate cancer cells causes chemoresistance and radioresistance and promotes tumor growth. Mol Cancer Ther 2010;9:336–46.

33. Sayin VI, LeBoeuf SE, Singh SX, Davidson SM, Biancur D, Guzelhan BS, et al. Activation of the NRF2 antioxidant program generates an imbalance in central carbon metabolism in cancer. eLife 2017;6:e28083.

34. Bar-Peled L, Kemper EK, Suciu RM, Vinogradova EV, Backus KM, Horning BD, et al. Chemical proteomics identifies druggable vulnerabilities in a genetically defined cancer. Cell 2017;171:696–709.

35. Tonelli C, Chio IIC, Tuveson DA. Transcriptional regulation by Nrf2. Antioxid Redox Signal 2018;29:1727–45.

36. Hayes JD, Dinkova-Kostova AT. The Nrf2 regulatory network provides an interface between redox and intermediary metabolism. Trends Biochem Sci 2014;39:199–218.

37. Momcilovic M, Bailey ST, Lee JT, Fishbein MC, Braas D, Go J, et al. The GSK3 signaling axis regulates adaptive glutamine metabolism in lung squamous cell carcinoma. Cancer Cell 2018;33:905–21.

38. Xiang Y, Stine ZE, Xia J, Lu Y, O'Connor RS, Altman BJ, et al. Targeted inhibition of tumor-specific glutaminase diminishes cell-autonomous tumorigenesis. J Clin Invest 2015;125:2293–306.

39. DeBerardinis RJ, Mancuso A, Daikhin E, Nissim I, Yudkoff M, Wehrli S, et al. Beyond aerobic glycolysis: transformed cells can engage in glutamine metabolism that exceeds the requirement for protein and nucleotide synthesis. Proc Natl Acad Sci U S A 2007;104:19345–50.

40. Wise DR, Thompson CB. Glutamine addiction: a new therapeutic target in cancer. Trends Biochem Sci 2010;35:427–33.

41. Brunelli L, Caiola E, Marabese M, Broggini M, Pastorelli R. Capturing the metabolomic diversity of KRAS mutants in non-small-cell lung cancer cells. Oncotarget 2014;5:4722–31.

42. Brunelli L, Caiola E, Marabese M, Broggini M, Pastorelli R. Comparative metabolomics profiling of isogenic KRAS wild type and mutant NSCLC cells in vitro and in vivo. Sci Rep 2016;6:28398.

43. Son J, Lyssiotis CA, Ying H, Wang X, Hua S, Ligorio M, et al. Glutamine supports pancreatic cancer growth through a KRAS-regulated metabolic pathway. Nature 2013;496:101–5.

44. Gaglio D, Metallo CM, Gameiro PA, Hiller K, Danna LS, Balestrieri C, et al. Oncogenic KRas decouples glucose and glutamine metabolism to support cancer cell growth. Mol Syst Biol 2011;7.

45. Kawada K, Toda K, Sakai Y. Targeting metabolic reprogramming in KRAS-driven cancers. Int J Clin Oncol 2017;22:651–59.

46. Faubert B, Vincent EE, Griss T, Samborska B, Izreig S, Svensson RU, et al. Loss of the tumor suppressor LKB1 promotes metabolic reprogramming of cancer cells via HIF-1α. Proc Natl Acad Sci U S A 2014;111:2554–9.

47. Parker SJ, Svensson RU, Divakaruni AS, Lefebvre AE, Murphy AN, Shaw RJ, et al. LKB1 promotes metabolic flexibility in response to energy stress. Metab Eng 2016;43:208–17.
48. Goodwin J, Neugent ML, Lee SY, Choe JH, Choi H, Jenkins DMR, et al. The distinct metabolic phenotype of lung squamous cell carcinoma defines selective vulnerability to glycolytic inhibition. Nat Commun 2017;8: 15503.
49. Momcilovic M, McMickle R, Abt E, Seki A, Simko SA, Magyar C, et al. Heightening energetic stress selectively targets LKB1-deficient non–small cell lung cancers. Cancer Res 2015;75:4910–22.
50. Heiss EH, Schachner D, Zimmermann K, Dirsch VM. Glucose availability is a decisive factor for Nrf2-mediated gene expression. Redox Biol 2013;1: 359–65.
51. Khamari R, Trinh A, Gabert PE, Corazao-Rozas P, Riveros-Cruz S, Balayssac S, et al. Glucose metabolism and NRF2 coordinate the antioxidant response in melanoma resistant to MAPK inhibitors. Cell Death Dis 2018;9:325.
52. Liu Y, Marks K, Cowley GS, Carretero J, Liu Q, Nieland TJF, et al. Metabolic and functional genomic studies identify deoxythymidylate kinase as a target in LKB1-mutant lung cancer. Cancer Discov 2013;3:870–9.
53. Cheng T, Sudderth J, Yang C, Mullen AR, Jin ES, Matés JM, et al. Pyruvate carboxylase is required for glutamine-independent growth of tumor cells. Proc Natl Acad Sci U S A 2011;108:8674–9.
54. Yang C, Ko B, Hensley Christopher T, Jiang L, Wasti Ajla T, Kim J, et al. Glutamine oxidation maintains the TCA cycle and cell survival during impaired mitochondrial pyruvate transport. Mol Cell 2014;56:414–24.
55. Daemen A, Liu B, Song K, Kwong M, Gao M, Hong R, et al. Pan-cancer metabolic signature predicts codependency on glutaminase and de novo glutathione synthesis linked to a high-mesenchymal cell state. Cell Metab 2018;28:383–99.